NTNU

Norwegian University of
Science and Technology

# Understanding the Effect of Porosity of Cu:SAPO-34 and AgCu:SAPO-34 for the HC-SCR deNOx Reaction

**Ellen-Margrethe Meberg Schjetlein**

Master of Science

Submission date: June 2018

Supervisor: Karina Mathisen, IKJ

Co-supervisor: Tina Kristiansen, IKJ
Guro Sørli, IKJ

Norwegian University of Science and Technology
Department of Chemistry

# Understanding the effect of porosity of Cu:SAPO-34 and AgCu:SAPO-34 for the HC-SCR deNOx reaction

Ellen-Margrethe Meberg Schjetlein

Master thesis

01.06.2018

# Acknowledgements

The work of this thesis was carried out at the Department of Chemistry at the Norwegian University of Science and Technology (NTNU) in Trondheim, and represent the end of my five years at NTNU.

Firstly, I want to thank my supervisor, Dr.Karina Mathisen, for her guidance and support. I would also thank my co-supervisors PhD. Candidate Guro Sørli and Post. Doc Tina Kristiansen for helping me in the lab, answering all my questions and making the time for me when I needed it. I would also like to thank PhD. Candidate Stian Forselv for providing me with a sample important to my work.

The rest of my research group also deserve thanks. Especially the weekly group meetings with quizzes and the awesome trip to Røros made this semester memorable.

I would like to thank my classmates for making me forget my worries during the daily lunchbreak. At last I would like to thank Johannes for supporting me, comforting me, and making me believe in myself when I didn't.

# Sammendrag

Dette er en masteroppgave som går videre på arbeid gjort av Botne (2017)[1]. SAPO-34 med forskjellig porøsitet ble ionebyttet med kobber samt ko-ionebyttet med både kobber og sølv. Materialene ble testet for reaksjonen selektiv katalytisk reduksjon av NO og $NO_2$ (samlebetegnelse NOx) med propen som reduktant. Hierarkisk SAPO-med innkorporert kobber ble forsøkt syntetisert, uten suksess. Krystalliniteten av SAPO-34, Cu:SAPO-34, AgCu:SAPO-34 og CuSAPO-34 ble verifisert med Røntgendiffraksjon (XRD), og overflateareal samt porestørrelser ble målt ved hjelp av Brunauer- Emmett- Teller (BET)- og Barett, Joyner and Halenda (BJH)-metoden. Innholdet av metall ble detektert ved hjelp av Inductively Coupled plasma - Mass Spectrometry (ICP-MS). Konversjonen av NOx (deNOx) ble målt ved hjelp av en Chemiluminecence NO/NOx analyzer i tørr og våt føde.

Et kjent problem er at SAPO-34 ionebyttet med kobber ofte kollapser[2], noe Botne (2017)[1] opplevde. I denne oppgaven, ble dette unngått ved å gjøre ionebyttingen i to steg, og alle prøvene bortsett fra en var aktive for (HC-SCR-)deNOx. Prøven med høyest oppnådd konversjon, var den konvensjonelle Cu:SAPO-34 i tørr føde som nådde 70% konversjon ved 375°C. Hierarkisk og konversjonell Cu:SAPO-34 skilte seg ikke veldig fra hverandre i denne studien, med forhåndsvis 58,3% versus 59,3% som høyeste konversjon i våt føde. Derimot var det stor forskjell på hierarkisk og konvensjonell AgCu:SAPO-34 i tørr føde, med forhåndsvis 54,2% versus 16,1% som høyeste konversjon. Våt føde utgjorde ikke store forskjeller, rundt 10 prosentpoeng ved liknende prøver. Bortsett fra èn prøve, var alle prøvene aktive i et bredere temperatur-intervall enn rapportert ved lignende prøver av Botne, i tillegg til at maksimum konversjon var oppnådd ved lavere temperaturer i denne studien.

# Abstract

This thesis is a continuation of another thesis written by Botne (2017)[1]. SAPO-34 with different porosity was ion-exchanged with copper and co-exchanged with copper and silver. The materials were tested for selective catalytic reduction (SCR) of NOx, with propene as reductant. An attempt was made to make samples with incorporated copper, with no success. The crystallinity of SAPO-34, Cu:SAPO-34, AgCu:SAPO-34 and CuSAPO-34 were verified with X-ray diffraction (XRD) and surface area and pore size were measured using Brunauer-Emmett-Teller (BET)- and Barett, Joyner and Halenda (BJH)- method. The metal content was detected with Inductively Coupled Plasma – Mass Spectrometry (ICP-MS). The NOx conversion was measured using a Chemiluminecence NO/NOx analyser in both dry and wet feed.

Botne (2017)[1] enlightened a known issue with structural collapse of SAPO-34, due to irreversible hydrolysis of Cu:SAPO-34 during the ion-exchange process.[3] In this thesis. this was prevented by doing the ion-exchange in two steps. All of the samples but one was active in the deNOx reaction, and the sample which achieved the highest conversion was the conventional Cu:SAPO-34 in a dry feed, reaching a conversion of 70% at 375°C. The hierarchical and conventional Cu:SAPO-34 in a wet feed were very similar, with 58.3% versus 59.3% as maximum conversion, respectively. Between hierarchical and conventional AgCu:SAPO-34 in a dry feed, the difference was respectively 54.2% versus 16.1%. Comparing similar samples, the wet feed did not impact the conversions more than about 10 percentage points. All but one of the samples was active in a broader temperature-range than reported with similar samples by Botne, and in this study the highest conversions was reached at lower temperatures.

# Abbreviations

A/F – Air-to-fuel ratio

AFI – Framework type

BET – Brunauer-Emmett-Teller

BJH – Barett, Joyner and Halenda

CHA – Zeolite framework type code (Chabazite)

CO – Carbon monoxide

DeNOx – The conversion of NOx

EEA – European Environment Agency

EPA – The Environmental Protection Agency

GC-MS – Chromatograph mass spectrometer

HC – Hydrocarbon

HC-SCR – Selevtive catalytic reduction with hydrocarbons

ICP-MS – inductively coupled plasma - mass spectrometry

MFC – Mass flow controller

m/z – Mass-to-charge ratio

NOx – NO and $NO_2$

NTNU – Norwegian University of Science and Technology

SAPO – Silicoaluminophosphates

SDA – Structure directing agent

TWCs – Three-way catalysts

UV – Ultraviolet

UNFCCC – United Nations Framework Convention on Climate Change)

VOC – Volatile organic compounds (VOCs)

wt% – Weight percent

XRD – X-ray diffraction

ZSM – Zeolite Socony Mobil

Å – Ångstrom

# Table of content

**Acknowledgements** **3**

**Sammendrag** **4**

**Abstract** **5**

**Abbreviations** **7**

**Table of content** **8**

**1.0 Introduction** **11**

**2.0 Theory** **15**

*2.1 NOx* *15*

*2.2 Hydrocarbon selective catalytic reduction* *16*

*2.3 Materials* *17*

2.3.1 SAPO-34 17

2.3.2 Hierarchical SAPO-34 19

2.3.3 Ion-exchange of SAPO-34 21

2.3.4 Incorporation of copper to SAPO-34 23

*2.4 Powder X-ray diffraction* *24*

*2.5 Surface area and pore size measurements by the BET- and BHJ-method* *26*

*2.6 Inductively coupled plasma - mass spectrometry* *28*

**3.0 Experimental** **29**

*3.1 Synthesis* *29*

Conventional SAPO-34 30

Hierarchical SAPO-34 31

CuSAPO-34 32

*3.2 Two-step ion-exchange* *32*

*3.3: Direct ion-exchange* *34*

*3.3 Powder X-ray diffraction* *35*

*3.4 Porosity measurements using N2 adsorption-desorption isotherms* *35*

*3.5 Inductively coupled plasma - mass spectrometry* *35*

*3.6 HC-SCR-DeNOx* *36*

**4. Results** **39**

*4.1 XRD* *39*

4.1.1 Plain SAPO-34 39

Altered crystallization time 40

Altered Si/Al ratio 41

Overview: Crystallinity vs synthesis parameters of SAPO-34 42

*4.1.2 Cu:SAPO-34 and AgCu:SAPO-34* *43*

Direct method 43

Two-step method 44

Overview ion-exchanged SAPO-34 47

4.1.3 CuSAPO-34 48

*4.2 BET results* *49*

*4.3 ICP-MS results* *56*

*4.4 HC-SCR-deNOx catalytic measurements* *57*

**5.0 Discussion** **63**

**6.0 Conclusion** **69**

**7.0 Further work** **71**

**8.0 References** **73**

**9.0 Appendixes** **79**
*Appendix 1: Additional XRD results* *79*
*Appendix 2: Additional BET results* *81*

# 1.0 Introduction

Air pollution has become a global concern and a great threat to both human and the environment.[3] Air pollution is defined as enough undesired materials in the atmosphere to produce adverse health effects to living organisms and the environment.[3] The biggest source of urban air pollution is motorized road vehicles which emit gasses like NOx and hydrocarbons.[2] The increased emission will impact the environment negatively, and should be slowed down. [2] In 1996 studies show that air pollution in developing countries is leading to tens of thousands of deaths and billions of dollars in medical costs.[4] One of the severe medical issues that can be caused by NOx, is that NO can attach to hemoglobin in the blood, reducing the transport of oxygen around the body.[5] NOx gases can also lead to the formation of acid rain which can cause fish death, and can remove minerals and nutrition from the soil that threes and plants need to grow.[6] In 2016, 20% of the NOx emission in Norway was caused by road traffic.[7]

The Kyoto agreement commits its parties to reduce emission of the six most important greenhouse gases, including NOx .[1] The Kyoto agreement is linked to United Nations Framework Convention on Climate Change (UNFCCC), which has a long term goal to stabilize the amount of gasses in the atmosphere and prevent a crucial amount of anthropogenic interference with the climate.[8] Because of the environmental and health consequences if the parties don't reduce their emissions, it is important to do tests to monitor the progress.

In September 2015, the Environmental Protection Agency (EPA) found a software installed in many Volkswagen diesel cars in America. [1] This software could detect when the vehicle was tested, and then programming it to release less $NO_x$. When the test was completed, the $NO_x$ emissions turned back to normal, and this resulted in 40 times more NOx emitted than allowed in the US. This was later referred to as the Volkswagen scandal.[9] This shows that a better way to reduce NOx gas emmisions from diesel vehicles is necessary and highly topical.

To remove NOx gases, there are mainly two methods; stationary sources such as power plants, and heavy-duty vehicles use ammonia-SCR,[10] while gasoline engines in passenger vehicles use three-way catalysts (TWC). Ammonia-SCR is not well suited for passenger vehicles, as it requires an additional tank filled with the reducing agent ammonia, which can

leak.[11-12] This tank needs to be refilled frequently, making it dependent on the drivers concern for the environment. The TWCs are only used in gasoline cars, because it requires almost stoichiometric air-to-fuel(A/F) ratio, it is not a good fit in diesel cars which operates in lean burn conditions, i.e. engines with an oxygen rich atmosphere.[12-13] A more fuel-efficient technology would be preferred, both to achieve better fuel economy and reduce exhaust gas emissions.[10] Lean burn engines have up to 30% lower fuel consumption than the stochiometric engines, which makes it a more fuel-efficient technology.[14] For this reason, it would be preferred to have a good catalyst that would fit for diesel vehicles. For this reason, it would be preferred to have a good catalyst that would fit for diesel vehicles, rather than stop driving vehicles with diesel engines.[10]

One method for reducing NOx gas emission that has received a lot of attention, is selective catalytic reduction of NOx with hydrocarbons (HC-SCR).[15] For the HC-SCR, different types of hydrocarbons already present in the exhaust have been tested as reductants. [16 16]. Catalysts have been tested, and the most active catalysts were zeolite based. In the study of Lee et. al (2016)[12], their copper ion-exchanged ZMS-5 got around 95% conversion of NOx in dry feed at 350°C, with n-butan as the reductant. However, the hydrothermal stability of the Cu:ZSM-5 is poor.

This master thesis is a continuation of the work done in the master thesis by Botne (2017).[1] Botne (2017) which attempted to make a catalyst which could help get rid of NOx gas emission from diesel vehicles. The method used for this, was hydrocarbon selective catalytic reduction (HC-SCR) of NOx. Some of the catalysts made was silicoaluminophosphate-34 (SAPO-34) with different porosity, both with only micropores (conventional SAPO-34), and with both micropores and mesopores (hierarchical SAPO-34). This thesis focus on hierarchical and conventional SAPO-34-and aims to further investigate aspects of HC-SCR-deNOx with copper ion-exchanged SAPO-34 along with silver and copper co-exchanged SAPO-34 as the catalyst, and propen as the reductant.

A major known problem[2], also experienced by Botne (2017)[1], was the collapse of Cu:SAPO-34 during ion-exchange, due to irreversible hydrolysis. [16] An important aspect in this thesis it therefore to investigate a method to prevent the irreversible hydrolysis. The HC-SCR-deNOx reactions done in Botne's thesis, are only done in dry feed, but in this thesis the hydrothermal

stability of SAPO-34 is tested by doing the deNOx in a wet feed, in addition to dry feed. An attempt was also made to incorporate SAPO-34 with copper.

This thesis starts by providing the necessary theory which cover the problems caused by NOx gas, some methods to reduce NOx gas emissions, materials used in this thesis, and the different characterization methods used which are powder XRD, surface measurements and ICP-MS. The theory is followed by the experimental part, which explains the methods for synthesis, ion-exchange, the characterizing methods and the catalytic reduction of NOx with the synthesized samples. The results are then presented before they are discussed, and finally there will be a conclusion.

# 2.0 Theory

## 2.1 NOx

NOx gases are an important factor for air quality, tropospheric chemistry, and the climate.[17] NOx can come from natural sources, such as biogenic emissions from bacteria in soils, biomass burning, and lightning strikes. There is also anthropogenic sources of NOx, such as fossil fuel combustion, biofuel combustion, emissions from vehicle transport, and industrial emissions.[17] Figure 2.1 shows the NOx emission sources in EU per. 2011 provided by European Environment Agency (EEA), where it is shown that the main source of NOx gases (40%) are road transport.

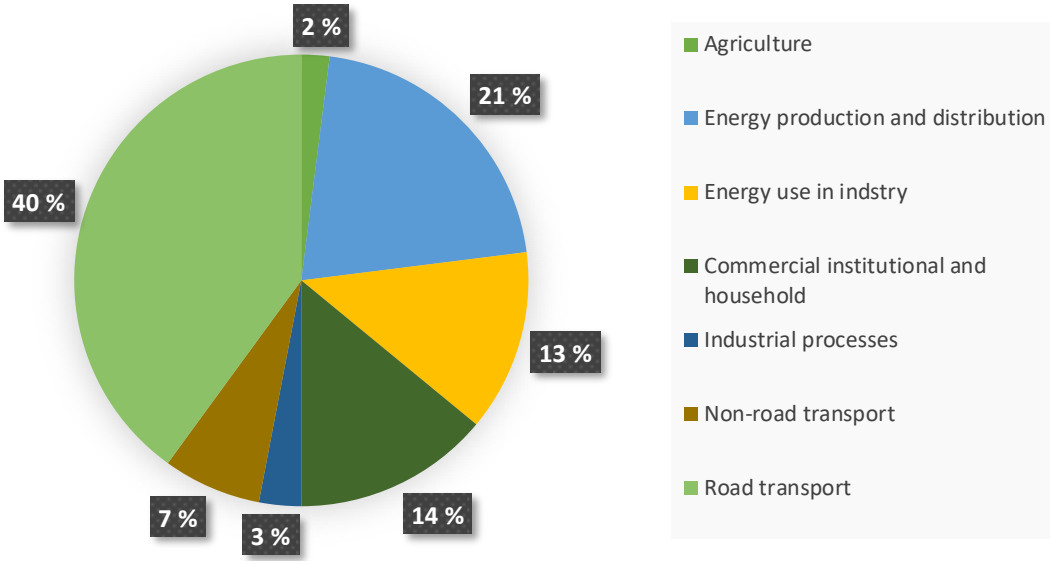


*Figure 2.1 NOx emission sources in the EU, 2011. Data sources is provided from European Environment Agency (EEA).*[18]

When NOx gases are in the presence of hydrocarbons, carbon monoxide (CO) and ultraviolet (UV) light, ground level ozone can be produced[15] Together with CO, volatile organic compounds (VOCs), and heat from the sunlight, the NOx gases can form smog. Smog and ground level ozone can lead to respiratory problems, making NOx emissions emissions both an environmental and a health issue.[19]

The toxicity of $NO_2$ is so severe it can cause burn in contact with skin and eyes. It can also cause inflammation of the airways (which is the principal mechanism of asthma[20]) and give reduced lung function. $NO_2$ is four times more toxic than NO for human health, but NO quickly oxidizes to $NO_2$.[10]

## 2.2 Hydrocarbon selective catalytic reduction

HC-SCR recieved a lot of attention, since it used a gas mixture similar to the gas found in exhausts. For HC-SCR, the reducing agent is hydrocarbon leftovers already present in the exhaust, so there is no need for an additional tank like ammonia-SCR needs.[12] In addition, the HC-SCR do not require a stoichiometric A/F ratio like TWC.[10, 12-13] The TWC needs the stochiometric A/F ratio since the oxidation of CO consumes too much CO under lean burn conditions, and the NOx conversion fails. The other way around, with lower oxygen the NOx is converted but the HC and CO are not completely oxidized.[21] Hence, HC-SCR seems to be a promising way to remove NOx gases in lean burn engines, provided that a suitable catalyst is developed.

In 1990, Iwamoto reported the first powerful catalyst for HC-SCR, copper ion-exchanged ZSM-5.[10] However, Cu:ZSM-5 exhibits poor stability in the presence of water at high temperatures. This is a problem, since water vapor is an inevitable component of lean burn engines emission. For better results for the HC-SCR, an alternative catalyst with high hydrothermal stability is needed.[23-24] SAPO materials, discovered in 1984, are molecular sieves that exhibit excellent hydrothermal stability.[22-23]

## 2.3 Materials

Zeolites are crystalline aluminosilicates which are porous on a molecular level, with structures containing channels and cavities. [24-26] Zeolites are composed of $TO_4$ tetrahedra (T= tetrahedrally coordinated atom, here Si and Al) with oxygen atoms connecting the neighbouring tetrahedra's. Zeotypes are zeolite-like materials containing other elements in addition to Si, Al and O, for example P.[24-26]

### 2.3.1 SAPO-34

SAPO-34 is a zeotype which share the topology of the natural zeolite chabazite (CHA).[27] The structure of chabazite is shown in Figure 2.2. SAPO-34 has a high surface area, Salmasi et.al (2012) reported the surface areas to be around 500 $m^2/g$- 600 $m^2/g$.[28] The pores and the high surface area gives excellent catalytic properties. [26-28] Micropores have a pore diameter below 20 Å, while mesopores have a diameter between 20Å and 500 Å.[27]

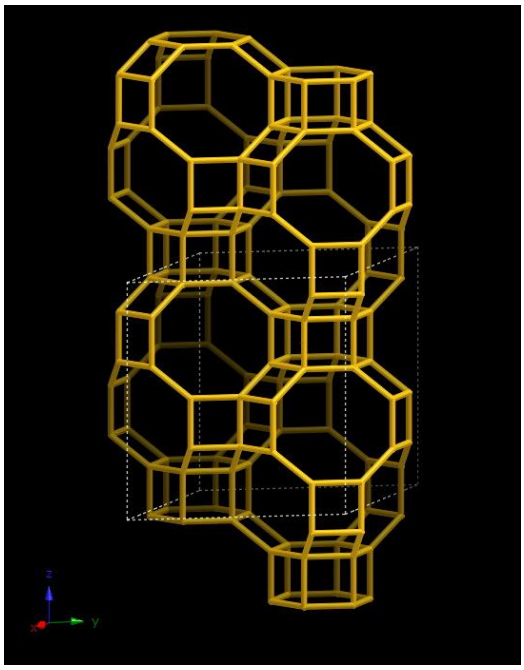

*Figure 2.2: Structure of the zeolite Chabazite. Copyright © 2017 Structure Commission of the International Zeolite Association.*[29]

SAPO-34 has a framework consisting of the T-atoms Si, Al, and P, with oxygen bridges between them.[27] The framework consists of an ABC ABC packing sequence of hexagonal prisms joined together by four-membered rings, resulting in a channel system and large ellipsoidal cages.[30] These ellipsoidal cages are about 11 Å long, and 6.5 Å wide. The cages are stacked hexagonally to form a three-dimensional network of cages, again linked by an eight-membered oxygen ring.[27, 30] The entrance to the cages is through the eight-membered oxygen ring with a diameter of approximately 3.8 Å, which make it possible to rapidly sorb molecules like for example $O_2$, $H_2$, $C_2H_6$, but excludes branched alkanes.[30]

In the synthesis of SAPO-34, SAPO-34 often compete to form with other structures.[31-32] The chabazite structure often compete with another structure called AFI, since the same templates are used in their synthesis. The SAPO-5 structure exhibits AFI topology, so a parallel formation of SAPO-34 and SAPO-5 phases often occur.

Different parameters could be changed to improve the selectivity towards the SAPO-34 structure on the expence of SAPO-5.[33-34] Both the crystallization time and the Si/Al ratio can have a effect on the formation of SAPO-34 instead of SAPO-5. Valizadeh et.al (2014) investigated the effect on crystallization time for SAPO-34 at 200 ºC. They reported that using longer crystallization time, 14 hours versus 6 hours, converted the SAPO-34 phase to SAPO-5 phase. [33] Li et.al. (2008) found that the amount of SAPO-5 increase with decreasing Si content.[4] In the study, SAPO-membranes with Si/Al ratio above 0.15 gave pure phase SAPO-34, and the SAPOs with Si/Al ratio 0.1 formed a mixture of SAPO-34 and SAPO-5.

### 2.3.2 Hierarchical SAPO-34

SAPO-34 can be obtained with different porosity.[36] Whereas conventional SAPO-34 exhibits only micropores, hierarchical SAPO-34 exhibits both micropores and mesopores. Hierarchical materials have less diffusion limitations than microporous materials. [33] The mesopores of hierarchical zeolites/zeotypes gives the advantage of fast mass transport, while in conventional zeolites/zeotypes there are diffusion limitations for transport of reagents with similar size as the micropores, or branched molecules. [36] Blocking of the pores, or coke, can be a problem in the narrow micropores since it leads to deactivation of the catalyst. To prevent the deactivation, mesopores can be introduced. The additional mesoporous network then improves the mass transport. The hierarchical materials can have a longer lifespan than the conventional materials, due to the increased mass transport because of the mesopores that can be much like “highways” in the materials.[35] These highways can improve the diffusional properties and speed up the traffic of reactants entering the catalyst, at the same time as products are attempting to exit.

To synthesize hierarchical SAPO-34, meso- structure directing agents (SDAs) are used as templates, in addition to the micro-SDA used during conventional SAPO-34 synthesis.[36]
This typically retain the microporous structure, but a mesoporous structure is also added. The difference with or without the meso-SDA can be seen in Figure 2.3. In the figure (a) and (b) are part of a conventional structure, while (c) and (d) are part of a hierarchical structure. (a) Shows a network of micropores, while (c) shows this network in addition to mesopores available from the surface. (b) Shows a nanostructure with microvoids, while (d) shows mesovoids in the middle a microporous network.

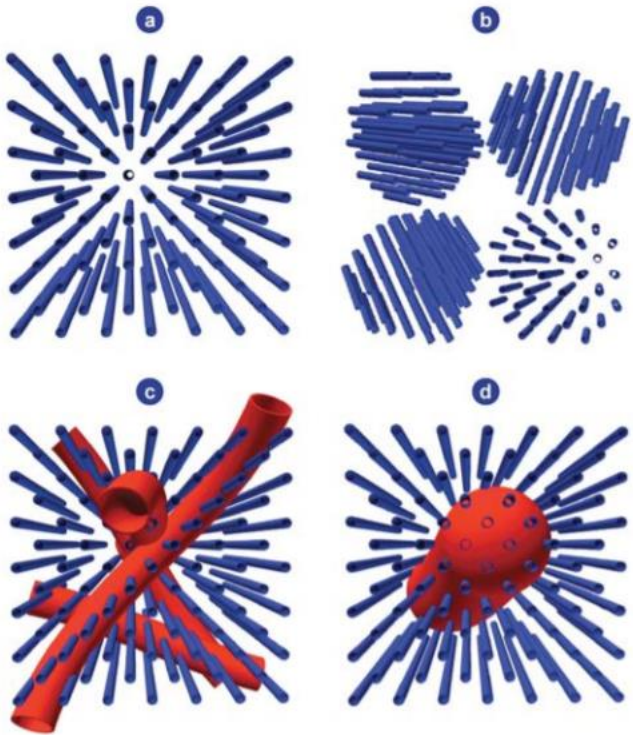


*Figure 2.3: Different framework of porous materials. (a) A microporous zeolite. (b) conventional framework with interparticle voids. (c) Mesopores available from surface in a network of micropores. (d) Mesovoids in the middle of the network of micropores. Reproduced from Chem. Soc. Rev., 2008, vol. 37, pages 2530-2542.*[37]

### 2.3.3 Ion-exchange of SAPO-34

There are three main methods that could be used to introduce cations to SAPO-34; ion-exchange, incorporation and impregnation. This thesis considers SAPO-34 ion-exchanged with copper (Cu:SAPO-34), co-exchanged with silver and copper (AgCu:SAPO-34), and incorporated with copper (CuSAPO-34).

The net framework charge of SAPO-34 is negative due to the phosphorus substitution by silicon, and formation of Bronsted acid sites ($H^+$) ions balance the charge. [22] Figure 2.4 shows a SAPO in this H-form. During the ion-exchange, the Bronsted acid sites are exchanged by a metal-ion cation. This can be done as in this thesis, with copper(II)ions and silver(I)ions. This makes SAPOs interesting for a number of catalytic reactions, for example reduction of $NO_x$ with hydrocarbons.[23]

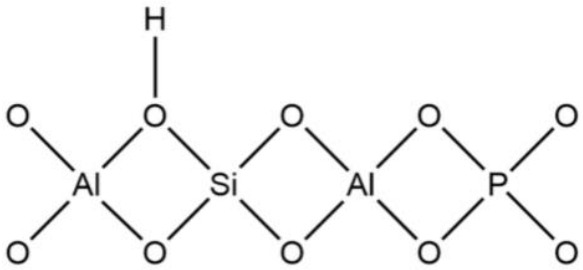


*Figure 2.4: SAPO in its H-form.*

Theoretically, the cations are placed on the cation sites in the structure of SAPO-34 when it is ion-exchanged.[27] The sites are shown in Figure 2.5, indicated by roman numerals. Site I is located from the 6-ring into the ellipsoidal cavity, where site II is located near the center. In the center of the hexagonal prism, site III is located, while site IV is placed near the 8-ring window.

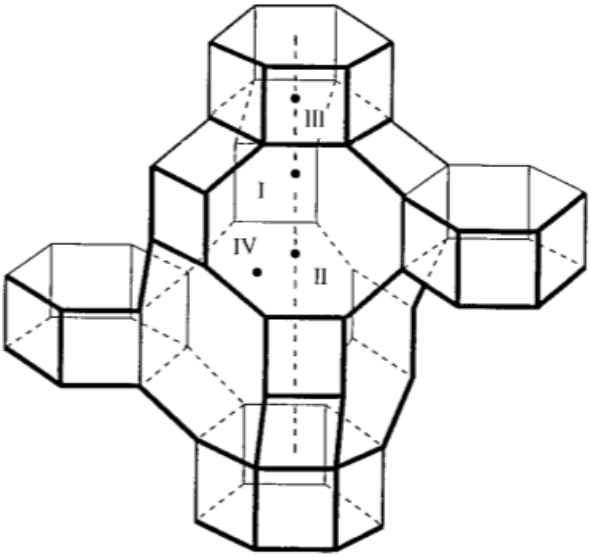


*Figure 2.5: SAPO-34, roman numerals indicates cation sites. The vertexes represent phosphorus, aluminium or silicon atoms, and the lines connecting them represents oxygen bridges. Reused with permission from Chemical Reviews; Vol 99, Hartmann, Kevan, Transition-Metal Ions in Aluminophosphate and Silicoaluminophosphate Molecular Sieves: Location, Interaction with Adsorbates and Catalytic Properties. Paged 635-664, Copyright 1999. American Chemical Society.*[27]

Unfortunately, SAPO-34 may undergo irreversible hydrolysis during ion-exchange of Cu, causing partial or complete structural collapse.[37] This problem is reported in a lot of studies, like Gao et. al. (2013)[38] and Xu. et. al. (2018).[2] This problem was also reported by Botne (2017)[1] with his conventional Cu:SAPO-34 in his master thesis[1]. The irreversible hydrolysis is shown in Figure 2.6. It shows that the Si-OH-Al bonds are exposed to the $H_2O$ attach, then the bonds are broken, and amorphous silicon complexes are formed.[37] However, the structural collapse can be avoided by ion exchanging SAPO-34 to ammonium form, according to Xu. Et.al (2017).[2] The ammonium species in $NH_4$-SAPO-34 could act as an important protection of the structure, preventing hydrolysis during a liquid Cu ion-exchange process.[2]

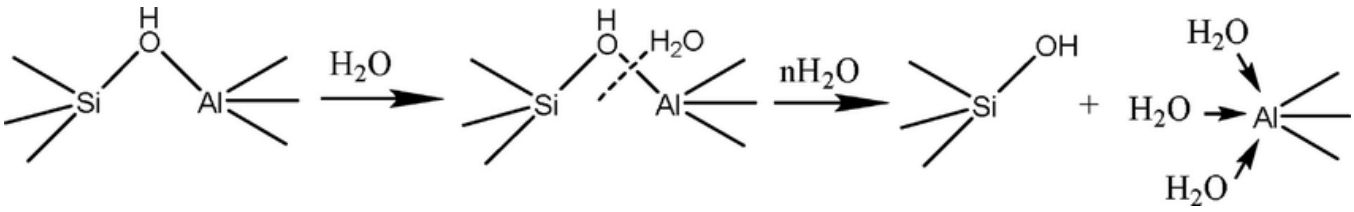


*Figure 2.6: The irreversible hydrolysis of SAPO-34, during ion-exchange. Taken with permission from: ResearchGate.*[2]

To improve the low-temperature hydrothermal stability of Cu:SAPO-34, silver has been used.[39] In the research of Xiang et. al. (2018), the ammonia-SCR, the Ag and Cu species did not interact, and the Ag species protected the SAPO-34 structure during the catalysis.[39]

### 2.3.4 Incorporation of copper to SAPO-34

In incorporation, the metal is directly incorporated into the framework by adding the copper source into the synthesis mixture.[27] Theoretically, the cations will go in to the tetrahedral framework bound to four oxygen atoms, and take the place of a tetrahedral atom.

## 2.4 Powder X-ray diffraction

XRD can be used to determine the structure of a sample and shows a fingerprint of the crystalline phases. [41-42] To do this, the sample is placed in a beam of X-rays and the X-ray diffractometer varies the angle from the plane on the surface. The diffracted X-rays Intensity(I) is measured as a function of the beam of the surface, θ.[40-41] The diffractogram can be used to detect the crystallinity of the sample, and can provide information about the composition of the crystalline phases present.[41] The phases present can be identified from computer search or a phase data library.[40] Sharp peaks in the diffractogram indicates a crystalline sample, while broad or no peaks indicates an amorphous sample. The emitted x-rays have an intensity proportional to the number of atoms, and their atomic number.

Since this thesis focus on SAPO-34, the diffractogram of Chabazite with the same peaks as SAPO-34 is shown in Figure 2.7.

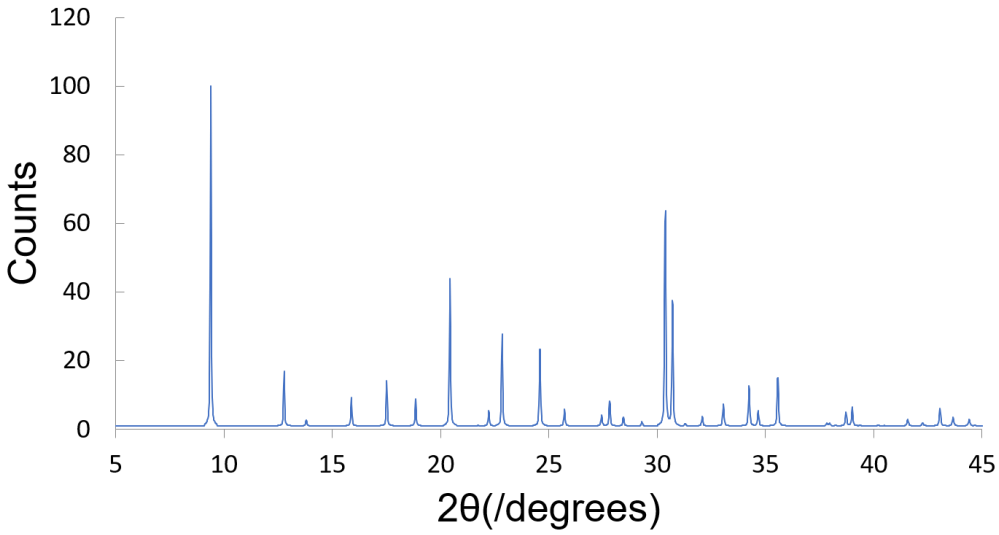


*Figure 2.7: Diffractogram of Chabazite. Taken with data from the database of zeolite structures.*[29]

As established in section 2.3.1, SAPO-34 competes with SAPO-5 with AFI topology. The diffractogram of AFI is shown in Figure 2.8.

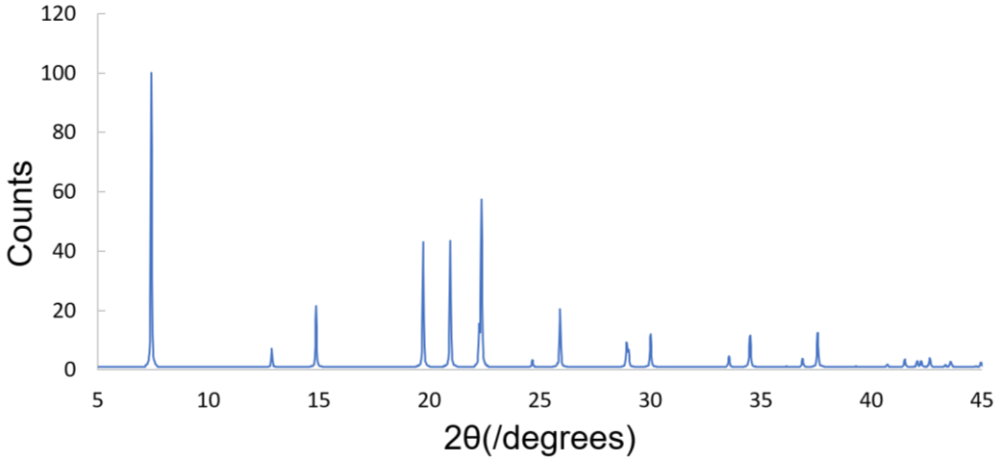


*Figure 2.8: Diffractogram of AFI. Taken with data from the database of zeolite structure.*[29]

## 2.5 Surface area and pore size measurements by the BET- and BHJ-method

Porosity, defined as the volume of the surface flaws with depth greater than the width, is drastically increasing the surface area.[42] The surface area is an important parameter of solid materials, due to the effect on reactivity. The surface area for porous materials can be measured with a gas adsorption technique such as BET. The gas used, often $N_2$, will be physically adsorbed on the surface of the solid, which means the sorbed molecules are free to cover the whole surface and are not bound to specific sites on the surface. The sorbent gas forms a monolayer on the surface, and repulsion from previously adsorbed gas makes it hard for a second layer to form.[42]

Theoretically the adsorption on the monolayer should stop when it is fully covered. In reality, additional molecules are adsorbed. [43] The ratio between partial pressure of the adsorbate in the gas, and vapor pressure of the pure adsorbate ( $\frac{P}{P_0}$ ) is important as it represents the activity of the adsorbate.[43] The sorption isotherm is a plot of amount of gas adsorbed at a constant temperature, against relative pressure.[42] This plot can be used to determine how much gas is needed to form the monolayer, thus measuring the surface area. The condensation in the pores at adsorption, is not at the same relative pressure as from the same pores at desorption. The isotherm from the adsorption and desorption can be combined, to usually form a hysteresis loop.[42] Figure 2.9 show the most common isotherms. Type I isotherm are normal for microporous adsorbents, types II, III, and VI can indicate nonporous or microporous materials, and types IV and V have hysteresis loops and are normal for mesoporous materials.

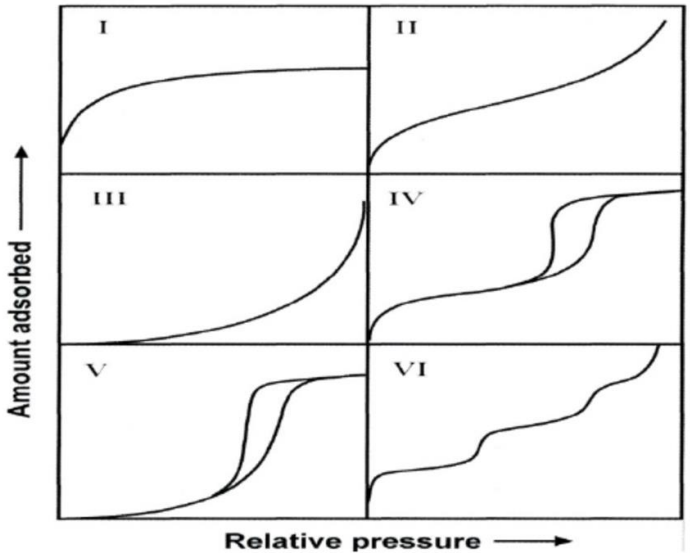


*Figure 2.9: The most common types of isotherm.*[44]

The different types of hysteresis loops, are shown in Figure 2.10. In the figure, H1 and H2 shows hysterisis loops that characterize two kinds of mesopore structures. H1 indicates uniform mesopore structure, while H2 indicates a complex pore structure with important network effects. H3 and H4 indicate no well-defined mesopores.

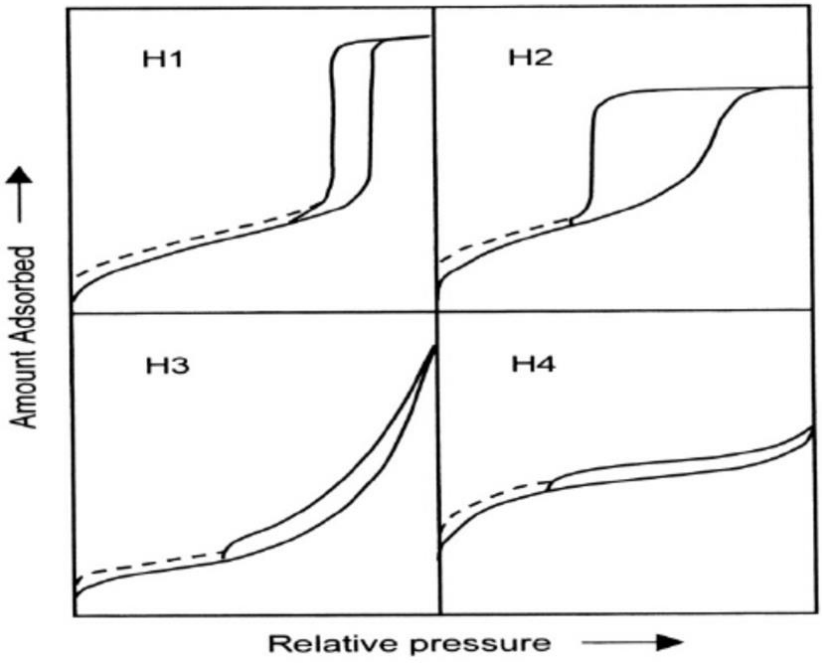


*Figure 2.10: The different types of hysterisis loops.*[44]

In addition to BET, BJH is often also done simultainously during the measurement.[45-46] It corrects the multilayer adsorption and is used to obtain the mesopore size distribution of the material. The procedure is based on the capillary condensation theory using the desorption of the isotherm, in addition to assuming a cylindrical geometry.[45-46]

## 2.6 Inductively coupled plasma - mass spectrometry

ICP-MS is an element analysis technique with the ability to precisely detect and measure trace elements in most materials.[47] The analytes pass through plasma and is ionized, then goes into a mass spectrometer (MS). The MS uses the mass-to-charge ratio (m/z) to determine a signal from each element, which is used to identify the elements and the isotopes. Since the m/z of different isotopes can be similar, the abundancy of each isotope must be carefully considered.

In this thesis, ICP-MS was used to detect the content of copper and/or silver in the ion-exchanged samples.

# 3.0 Experimental

## 3.1 Synthesis

In the syntheses, the sources of Al, Si and P were pseudoboehmite ($Al_2O_3$, 71,8%) obtained from Sasol North America, colloidal silica ($SiO_2$, 40%) obtained from Sigma Aldrich and phosphoric acid ($H_3PO_4$, 85%) obtained from Merck. For the copper incorporate SAPO-34, copper(II)oxide powder (CuO) obtained from VWR chemicals and tetraethylenepentamine (TEPA) obtained from Sigma Aldrich were used.

In the syntheses, the micro-SDAs used were:

- Triethylamine (TEA, 99%) obtained from Sigma Aldrich
- Tetraethylammonium hydroxide (TEAOH, 25 wt%) obtained from Sigma Aldrich
- Morpholine (MOR) obtained from Sigma Aldrich
- Tetramethylammonium hydroxide (TMAOH, 25 wt%) obtained from Sigma Aldrich
- Tetrapropylammonium hydroxide (TPAOH, 1.0 M) obtained from Sigma Aldrich

For the mesoporous SAPO-34, the meso-SDAs added were:

- Polyethylene oxide ( PEO, average $M_v$: 100000, 100%) obtained from Sigma Aldrich
- Cetyltrimethylammonium bromide (CTAB) obtained from Sigma Aldrich
- Poly (ethylene glycol)-block-poly(propylene glycol)-block-(polt\y(ethylene glycol) (P123, average $M_n$: 5800) obtained from Sigma Aldrich. Before P123 was added, it was diluted in etanol ($C_2H_6O$, 10mL, 100%) obtained from VWR chemicals
- Dimetyloctadecyl[3-(trimethoxysily)propyl]ammonium chloride (DMOD, 42 wt%) obtained from Sigma Aldrich
- Glucose ( GLU) obtained from Sigma Aldrich.

For the ion-exchanged samples, the source of copper and silver used were: Ammonium nitrate solution (27%, $(NH_4)(NO_3)$) obtained from VWR chemicals, copper (II) sulphate ($CuSO_4 \cdot 5H_2O$) obtained from Riedel-de Haën®, copper nitrate ($CuNO_3 \cdot 5H_2O$) obtained from Sigma Aldrich, silver nitrate ($AgNO_3$) obtained from VWR international, copper(II)nitrate ($Cu(NO_3)_2 \cdot H_2O$) obtained from Sigma Aldrich.
Additional chemicals used in the ion-exchange were concentrated ammonia ($NH_3$, 32%) obtained from Sigma Aldrich.

### Conventional SAPO-34

The different synthesises was done with the following molar ratios;

- 1 Al: 1 P: 0.4 Si: 1 TEA: 0.1 TEAOH: 0.05 meso SDA: 25 $H_2O$
- 1 Al: 1 P: 0.2 Si: 1 TEA: 0.1 TEAOH: 1 extra micro-SDA: 0.05 meso SDA: 25 $H_2O$

$H_3PO_4$ (7,9g) and water (x g) was added to a beaker. The amount of water had to be calculated according to the content of water in the chemicals used. The mixture was stirred, and $Al_2O_3$ (4,9 g) was added. CuO (2.07 g/ 4.14 g) was added, followed by the desired micro-SDAs (TEA, TEAOH and MOR). The amount of SDAs are calculated using the molar ratio. Then the mixture was stirred, followed by crystallization in the oven contained in an autoclave, varying from 24-120 hours using temperatures ranging from 150-180ºC. The resulting crystallized solid was filtrated and rinsed with deionized water.

Table 3.1 shows which SDAs is added to each sample, in addition to information about the acidity, crystallization time and temperature for the crystallization. In this thesis, S stands for SAPO-34, C stands for conventional.

*Table 3.1: Synthesis parameters for conventional SAPO-34: The Al:Si molar ratio, crystallization time, temperature and SDA.*

| Sample | Al:SI | Crystallization time (h) | Temp (ºC) | SDA |
|---|---|---|---|---|
| ConvS_01 | 1: 0.2 | 120 | 150 | TEA, TEAOH |
| ConvS_02 | 1: 0.2 | 120 | 150 | MOR |
| ConvS_03 | 1: 0.4 | 120 | 150 | TEA, TEAOH |

### Hierarchical SAPO-34

The syntheses of hierarchical SAPO-34 were similar to the conventional SAPO-34, but after the micro-SDAs were added, meso-SDAs were added (glucose, CTAB, DMOD, P123 and PEO). The type of meso-SDA that is added to each sample, is shown in the last column of Table 3.2. The table also contains information about the acidity, crystallization time and temperature for the crystallization. In this thesis, H stands for hierarchical.

*Table 3.2: Synthesis parameters for hierarchical SAPO-34: The Al:Si molar ratio, crystallization time, temperature and SDA.*

| Sample | Al:Si | Crystallization time (h) | Temp (°C) | SDA |
|---|---|---|---|---|
| HierS_01 | 1: 0.2 | 120 | 150 | TEAOH, GLU |
| HierS_02 | 1: 0.2 | 120 | 150 | MOR, CTAB |
| HierS_03 | 1: 0.2 | 120 | 150 | TEAOH, GLU |
| HierS_04 | 1: 0.2 | 72 | 180 | TEA, TEAOH, DMOD |
| HierS_05 | 1: 0.2 | 72 | 180 | TEA, TEAOH, CTAB |
| HierS_06 | 1: 0.2 | 72 | 180 | TEA, TEAOH, P123 |
| HierS_07 | 1: 0.2 | 72 | 180 | TEA, TEAOH, PEO |
| HierS_08 | 1: 0.4 | 72 | 180 | TEA, TEAOH, CTAB |
| HierS_09 | 1: 0.2 | 26 | 180 | TEA, TEAOH, DMOD |
| HierS_10 | 1: 0.2 | 26 | 180 | TEA, TEAOH, P123 |
| HierS_11 | 1: 0.2 | 26 | 180 | TEA, TEAOH, PEO |

### CuSAPO-34

In addition to the plain SAPO-34, copper incorporated SAPO-34 was synthesized.
The ratio of this synthesis was 1: Al: 1P: 0.5 Si: 0.5 micro SDA: 0.01 CuTEPA.

$H_3PO_4$ (7.96 g) and water (37.299 g) was added to a beaker. The mixture was stirred, and CuO (0.055g) was added. TEPA (0.124g) was added and the mixture was stirred for 30 minutes, then $Al_2O_3$ (4.9 g) was added. CuO (5.18 g) was added, followed by the desired micro-SDAs (TEAOH, TPAOH, TMAOH). The amount of SDAs are calculated using the molar ratio. Then meso-SDAs (CTAB, CTAOH) were added. Then the mixture was stirred, followed by crystallization in the oven, contained in a autoclave, varying from 120-240 hours, using temperatures ranging from 150-180ºC. The resulting crystallized solid was filtrated and rinsed with deionized water. Which SDAs used in each sample are shown in Table 3.3. In addition to this, the table provides information about the acidity, crystallization time, temperature for the crystallization. In this thesis, Cu stands for copper, and CuSAPO-34 is copper incorporated SAPO-34.

*Table 3.3: Synthesis parameters for the hierarchical CuSAPO-34: The Al:Si molar ratio, crystallization time, temperature and SDA.*

| Sample | Al:Si | Crystallization time (h) | Temp (ºC) | SDA |
|---|---|---|---|---|
| CuHierS_01 | 1: 0.5 | 120 | 150 | TMAOH, TPAOH, CTAB |
| CuHierS_02 | 1: 0.5 | 120 | 150 | TMAOH, TPAOH, CTAOH |
| CuHierS_03 | 1: 0.5 | 240 | 150 | TMAOH, TPAOH, CTAB |
| CuHierS_04 | 1: 0.5 | 120 | 150 | TMAOH, TEAOH, CTAOH, |
| CuHierS_05 | 1: 0.5 | 120 | 150 | TEAOH, CTAB |
| CuHierS_06 | 1: 0.5 | 120 | 150 | TEAOH, TPAOH, CTAOH |
| CuHierS_07 | 1: 0.5 | 120 | 150 | TMAOH, TEAOH, TPAOH, CTAB |

## 3.2 Two-step ion-exchange

In the two-step ion-exchange the SAPO-34 is ion-exchanged with ammonium before it is ion-exchanged with the metal cation, as shown in equation 3.1 and 3.2.

$$\text{SAPO-34} \rightarrow \text{NH}_4^+\text{/SAPO-34} \rightarrow \text{Cu:SAPO-34} \quad (3.1)$$

$$\text{SAPO-34} \rightarrow \text{NH}_4^+\text{/SAPO-34} \rightarrow \text{AgCu:SAPO-34} \quad (3.2)$$

SAPO-34 was first ion-exchanged with $NH_4^+$ by adding SAPO-34(1g) to an ammonium nitrate solution (100 mL, 27 wt%). The mixture was then stirred for two hours at 80°C. After the stirring, the solid was filtrated and rinsed with deionized water. $NH_4^+$/SAPO-34 was dried for 16 hours, at 70°C. Then this procedure was repeated.

To make Cu:SAPO-34, the $NH_4^+$/SAPO-34 powder made as above, was mixed with $CuSO_4$ solution (40 mL, 0.053 M). The mix was stirred for 12 hours at 70 °C. At last, the solid was filtrated and rinsed with deionized water. The solid was dried for 16 hours at 70°C.

For the AgCu:SAPO-34, the $NH_4^+$/SAPO-34 powder made as above, and mixed with a $CuNO_3$ solution (40 mL, 0.053 M). After the 12 hours of stirring, an $AgNO_3$ solution (40 mL, 0.126 M) was added to the mixture, and it was stirred for 16 hours. Then the solid was filtrated and dried like above.

### 3.3: Direct ion-exchange

The direct ion-exchange was done in one step, as shown in equation 3.3 and 3.4.

$$\text{SAPO-34} \rightarrow \text{Cu:SAPO-34} \quad (3.3)$$

$$\text{SAPO-34} \rightarrow \text{AgCu:SAPO-34} \quad (3.4)$$

The direct ion-exchanged Cu:SAPO-34 required a tetraamine copper(II) solution. To make this, a $Cu(NO_3)_2$ solution (1.812 g) was dissolved in deionized water (250 ml). Half of the solution was transferred to a beaker and let to stir. $NH_3$ was diluted with deionized water until the **c**oncentration was 5 M. Then, the ammonia solution was added to the copper(II)nitrate solution. The tetraamine copper(II) solution (30 mL) was added to a beaker containing SAPO-34 (1g). To make the AgCu:SAPO-34, an $AgNO_3$ solution (30 mL , 0.053 M,) was added to the beaker. The mixture was stirred in room temperature for 24 hours. The solid was filtrated and rinsed with deionized water, and dried at 70°C.

Table 3.4 shows all of the ion-exchanged samples and the amount of the source of copper and silver added. If the ion-exchanged sample was made by the direct or the two-step method, is also listed. In this thesis, Cu: stands for ion-exchanged with copper, AgCu: stands for ion-exchanged with both silver and copper. D stands for "direct method", referring to ion-exchange directly from H-form. The sample ConvS_00 is a plain conventional SAPO-34 provided by PhD candidate Stian Forselv with Si/Al = 0.2.

*Table 3.4: Method used for ion-exchanged samples, and the amount Cu and Ag source added.*

| Sample name | Method | $CuSO_4$ (g) | $CuNO_3$ (g) | $AgNO_3$(g) |
|---|---|---|---|---|
| Cu:ConvS_00D | Direct | – | 1.812 | |
| AgCu:ConvS_00D | Direct | – | 1.812 | 0.27 |
| Cu:ConvS_00 | Two-step | 0.532 | – | – |
| AgCu:ConvS_00 | Two-step | – | 0.515 | 0.85 |
| Cu:HierS_05 | Two-step | 0.555 | – | – |
| AgCu:HierS_05 | Two-step | – | 0.513 | 0.90 |
| Cu:HierS_01 | Two-step | 0.531 | – | – |
| AgCu:HierS_01 | Two-step | – | 0.515 | 0.87 |

### 3.3 Powder X-ray diffraction

D8 A25 DaVinci X-ray Diffractometer with CuKα radiation, and LynxEye™ SuperSpeed Detector was used. The divergence slit opened automatically, and the illuminated length on the sample always remained at 6 mm. The step length was 0.013 °/step. The program used scanned the 2θ values between 5 degrees and 60 degrees and lasted for 15 minutes.

### 3.4 Porosity measurements using N2 adsorption-desorption isotherms

Approximately 0.2 g of the sample was placed in a test tube for dehydration at 250 °C for 24 hours in vacuum prior to measurements.

A Micromeritics TriStar 3000 Surface Area and Porosity Analyzer was used to conduct surface area and pore size distribution measurements, calculated by the BET/BJH-method from $N_2$ adsorption-desorption isotherms, that used $N_2$ at - 196°C for the adsorption and desorption measurements.

### 3.5 Inductively coupled plasma - mass spectrometry

The analysis to verify the metal content of the ion-exchanged zeotypes was carried out by Syverin Lierhagen, using an Agilent 8800 ICP Triple Quad.

The preparation was done by adding 15-45 mg of the sample to a Teflon tube (25 mL). To dissolve the sample, $HNO_3$ (concentrated, 1.5 mL) was added, followed by HF (40 wt%, 0.5 g). Then, the sample is transferred to a Teflon vessel and diluted to 250 g. A 16 mL Teflon tube was rinsed with the sample solution three times and filled with the solution. For background corrections , three blank samples were added to the analyses.

## 3.6 HC-SCR-DeNOx

The experimental rig for the catalysis is shown in Figure 3.1. HC-SCR-deNOx catalytic measurements was conducted using a CLD 62 Eco-Physics Chemiluminescence NO/NOx connected to a Nabertherm R50/250/12 tube furnace with a C450 controller, a Bronkhorst mass flow controller (MFC) controlled by a computer, chromatograph mass spectrometer (GC-MS) for analyzation of the outlet. The sample was held in place in a reaction tube inside the furnace. The composition of the feed gas was NO (2000 ppm), $O_2$ (10%), propene (2%), in addition to argon as the inert gas. $H_2O$ (10%) was added to the gas feed in two of the experiments using a bubbler.

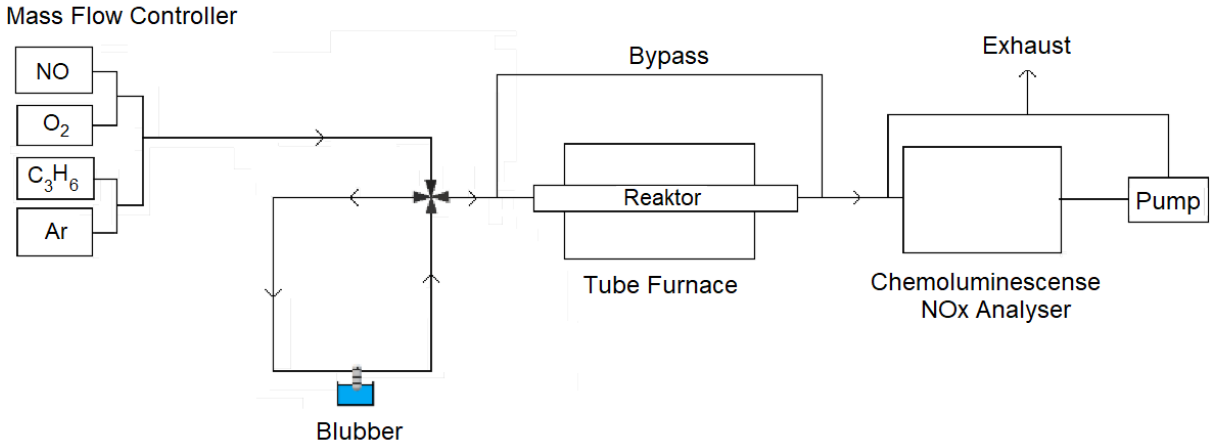


*Figure 3.1: The experimental rig for the catalytic testing.*

The samples were prepared to yield a particle size between 212 µm and 425 µm. This was achieved by first pressing the sample to a pellet, then added to a mortar. Then, the sample was transferred to three sieves with different openings, to achieve the right particle size.

0.150 g sample was placed in the metal tube reactor and,- kept in place with quartz wool to allow gas to flow freely through the sample.

The samples were heated up to 500°C in argon flow (5 mL/min) in a tube oven. The temperature program and concentrations used are illustrated in Figure 3.2. At 500°C, the sample was activated with an 80 mL/min, 2% $O_2$ and 98% Ar for an hour. After 60 minutes, the feed gas was set to 140 mL/min; 2% $O_2$, 1200 ppm propene and 2000 ppm NO. The feed gas was switched to a bypass line, flow until stable, to measure [NO] at bypass. Then the flow was set to go  through the sample. The conversion of NOx was measured in 25°C steps for 20 minutes, between 500°C and 275°C. The feed gas in the bypass line was measured again at 275°C.

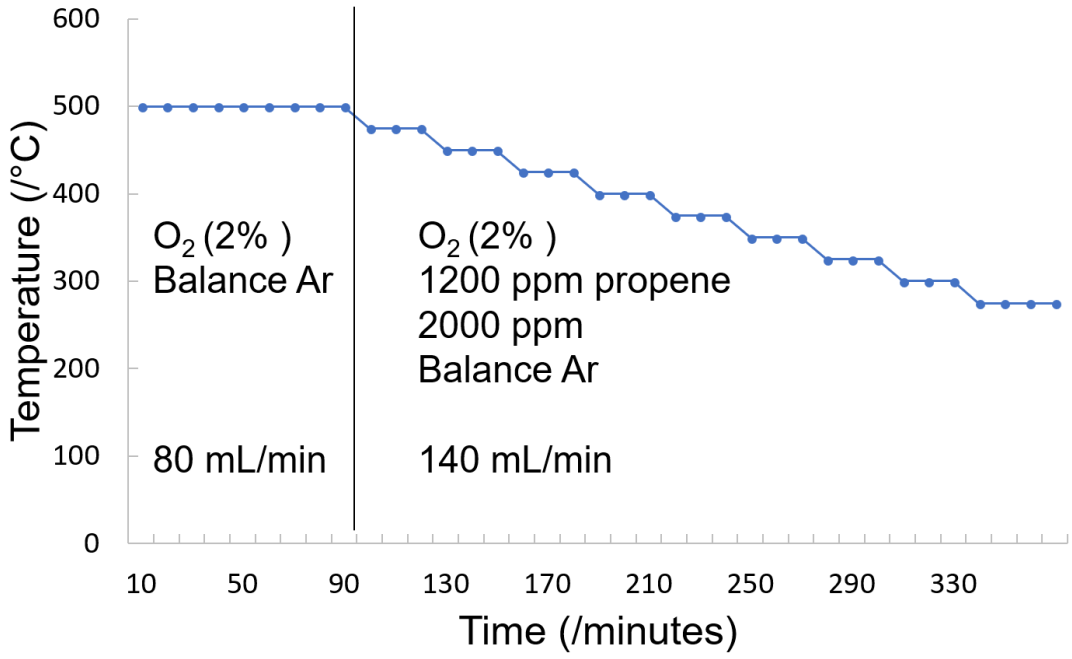


*Figure 3.2: Temperature program and concentrations used during the HC-SCR-deNOx.*

# 4. Results

## 4.1 XRD

### 4.1.1 Plain SAPO-34

14 Syntheses of plain SAPO-34 were done, three with only micro-SDAs, and 11 with both micro-SDAs and meso-SDAs. Of the 14 syntheses, only two samples were phase pure SAPO-34; ConvS_01 and HierS_05. Figure 4.1 show the diffractograms of the calcined HierS_05 and calcined ConvS_01 compared to chabazite. The diffractograms of the additional samples is shown in the appendix.

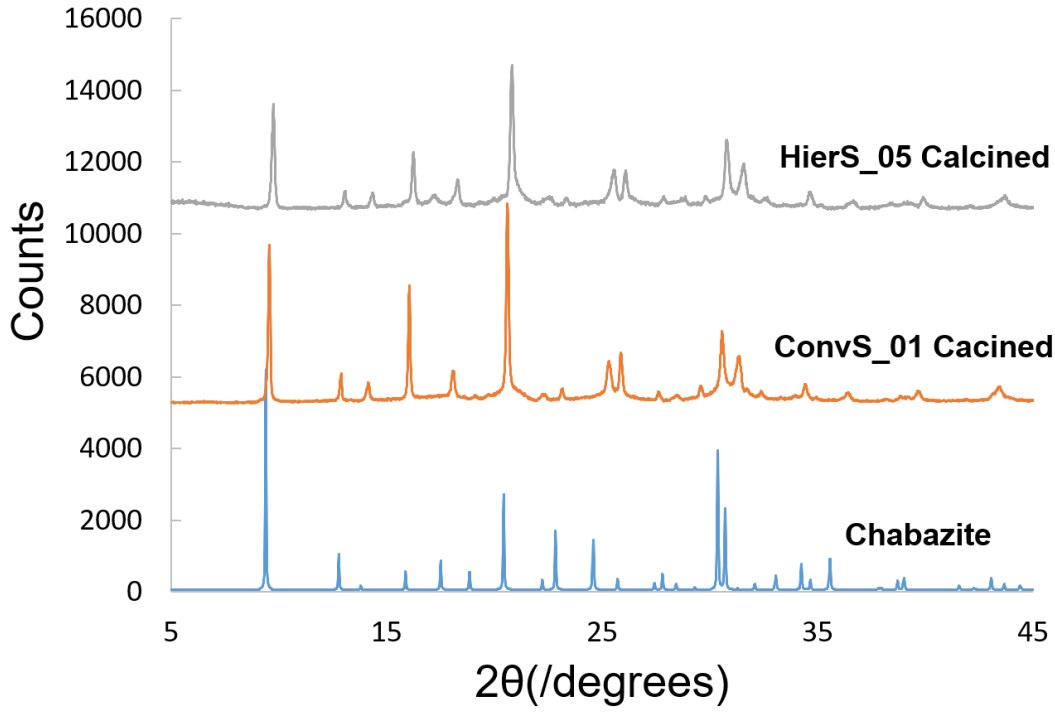


*Figure 4.1: Diffractograms of HierS_05 calcined and ConvS_01 calcined, compared to chabazite.*

### Altered crystallization time

To aim for more pure phase SAPO-34, five samples were re-synthesized with one parameter changed, the Si/Al ratio and crystallization time. For three samples, HierS_04, HierS_06 and HierS_07, the crystallization time was shortened from 72 hours to 26 as suggested in the study of Valizadeh et.al (2014)[33]. The resulting samples were HierS_09, HierS_10, HierS_11. An overview of the samples and their parameters, in addition to the XRD-results, can be seen in Table 4.1.

*Table 4.1: The original samples with 72 hours crystallization time, and the new samples with 26 hours crystallization. The XRD conclusions for the new samples are also listed.*

| Original sample | Crystallization time (h) | New sample | Crystallization time (h) | XRD conclusions new samples |
|---|---|---|---|---|
| HierS_04 | 72 | HierS_09 | 26 | CHA+AFI |
| HierS_06 | 72 | HierS_10 | 26 | CHA+AFI |
| HierS_07 | 72 | HierS_11 | 26 | CHA+AFI |

The XRD-results of the as prepared samples with shortened crystallization time are listed in Table 4.1, and the diffractograms are showed in Figure 4.2. The diffractograms are all matching a mixture of SAPO-5 and SAPO-34, despite shorter crystallization time.

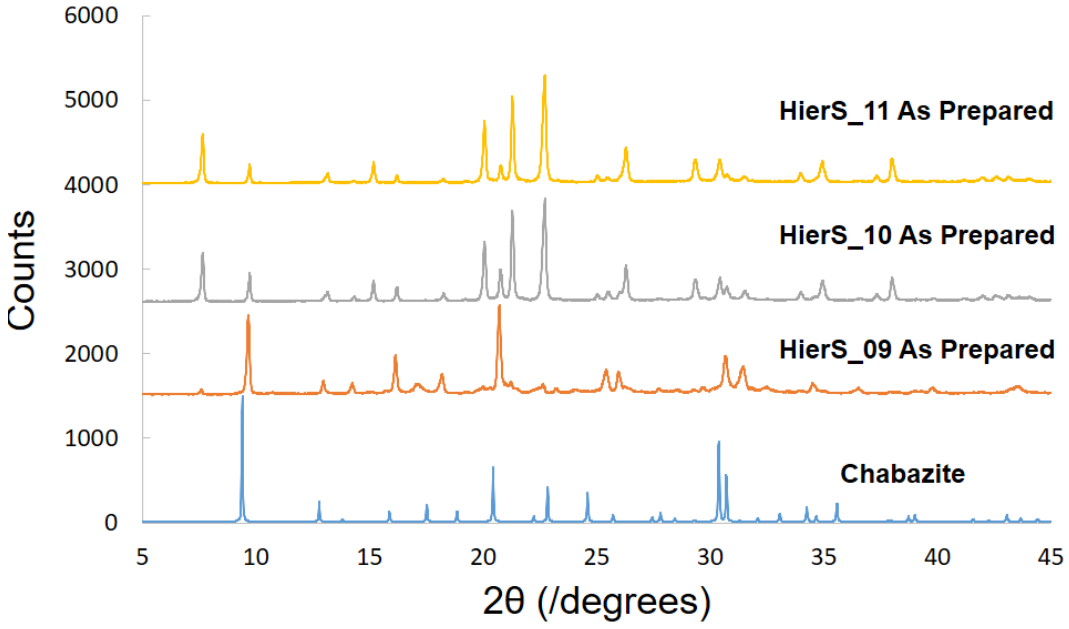


Figure 4.2: As prepared HierS_09, HierS_10, HierS_11, samples with shortened crystallization time.

### Altered Si/Al ratio

Two more samples were also re-synthesized with one parameter changed (increased Si/Al ratio), the phase pure HierS_05 and ConvS_01. For the new samples, HierS_08 and ConvS_03, the Si/Al ratio were increased from 0.2 to 0.4 as suggested in the study of Li et.al. (2008).[34] An overview of the samples and their parameters, in addition to the XRD-results, can be seen in Table 4.2.

*Table 4.2: Original samples with 1Al: 0.2Si, and the new samples with 1Al: 0.4Si. The XRD conclusions for the new samples are also listed.*

| Original sample | Al: Si | New sample | Al:Si | XRD conclusions new samples |
|---|---|---|---|---|
| HierS_04 | 1: 0.2 | HierS_09 | 1: 0.4 | CHA+AFI |
| HierS_06 | 1: 0.2 | HierS_10 | 1: 0.4 | CHA+AFI |
| HierS_07 | 1: 0.2 | HierS_11 | 1: 0.4 | CHA+AFI |

The XRD-results of the samples with changed crystallization time are listed in Table 4.2, and the diffractograms of the as prepared samples are showed in Figure 4.3. The diffractograms shows that the samples had peaks matching a mixture of SAPO-5 and SAPO-34.

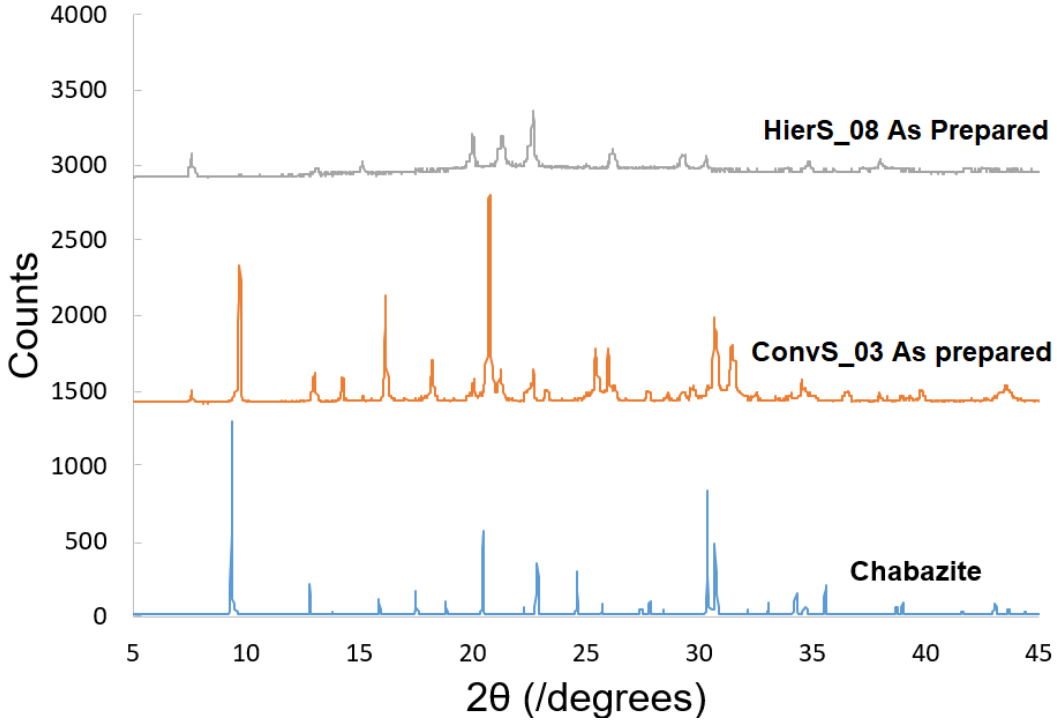


*Figure 4.3: Diffractograms of as prepared HierS_08 and ConvS_03.*

### Overview: Crystallinity vs synthesis parameters of SAPO-34

The XRD- results for all of the synthesized SAPO-34 are gathered in Table 4.3. The table also contains information about the acidity, crystallization time, temperature for the crystallization and the SDAs. The diffractograms of the synthesized SAPO-34 that are not provided, are shown in the appendix and were not pure phased SAPO-34.

*Table 4.3: XRD conclusions of the mentioned synthesized samples, in addition to already provided information about the samples.*

| Sample | Al:Si | Crystallization time (h) | Temp (°C) | SDA | XRD conclusion |
|---|---|---|---|---|---|
| ConvS_01 | 1: 0.2 | 120 | 150 | TEA, TEAOH | CHA |
| ConvS_02 | 1: 0.2 | 120 | 150 | MOR | AFI + CHA |
| ConvS_03 | 1:0.4 | 120 | 150 | TEA, TEAOH | AFI + CHA |
| HierS_04 | 1: 0.2 | 72 | 150 | TEA, TEAOH, DMOD | AFI + CHA |
| HierS_05 | 1: 0.2 | 72 | 180 | TEA, TEAOH, CTAB | CHA |
| HierS_01 | 1: 0.2 | 120 | 150 | TEAOH, GLU | AFI+CHA |
| HierS_02 | 1: 0.2 | 120 | 150 | MOR, CTAB | AFI + CHA |
| HierS_03 | 1: 0.2 | 120 | 150 | TEAOH, GLU | AFI + CHA |
| HierS_06 | 1: 0.2 | 72 | 180 | TEA, TEAOH, P123 | AFI + CHA |
| HierS_07 | 1: 0.2 | 72 | 180 | TEA, TEAOH, PEO | AFI + CHA |
| HierS_08 | 1:0.4 | 72 | 180 | TEA, TEAOH, CTAB | AFI + CHA |
| HierS_09 | 1: 0.2 | 26 | 150 | TEA, TEAOH, DMOD | AFI + CHA |
| HierS_10 | 1: 0.2 | 26 | 180 | TEA, TEAOH, P123 | AFI + CHA |
| HierS_11 | 1: 0.2 | 26 | 180 | TEA, TEAOH, PEO | AFI + CHA |

### 4.1.2 Cu:SAPO-34 and AgCu:SAPO-34

For the ion-exchange, the plain SAPOs used were: The hierarchical HierS_05, the conventional ConvS_01 and the conventional sample given by Stian Forselv, ConvS_00.

#### Direct method

Two samples were ion-exchanged directly, Cu:ConvS_00D and AgCu:ConvS_00D. They are listed along with the plain SAPO-34 used and the XRD-results in Table 4.4.

*Table 4.4: Samples ion-exchanged with the direct method, their precursor SAPO-34 and their XRD conclutions.*

| Sample | Plain SAPO-34 | XRD conclusion |
|---|---|---|
| Cu:ConvS_00D | ConvS_00 | Amorph |
| AgCu:ConvS_00D | ConvS_00 | CHA |

Their diffractograms compared to the plain SAPO-34 used, ConvS_00, are shown in Figure 4.4. The diffractograms shows that Ag:ConvS_00D is crystalline, while the sample Cu:ConvS_00D has almost collapsed and is amorph. The crystalline Ag:ConvS_00D has a much lower intensity than the calcined plain ConvS_00.

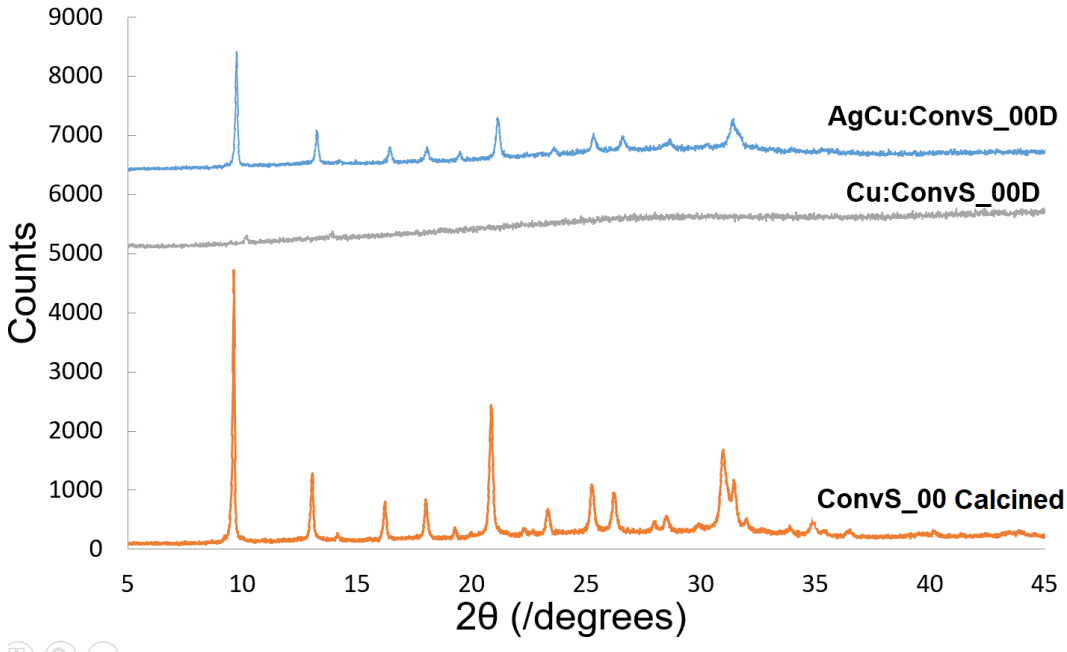


*Figure 4.4: Diffractograms of the plain SAPO-34 ConvS_00, and the ion-exchanged AgCu:ConvS_00D and Cu:ConvS_00D SAPO-34 samples.*

### Two-step method

Six samples were ion-exchanged directly, they are listed along with the plain SAPO-34 used and the XRD-results in Table 4.5. Three of them were ion-exchanged with copper; Cu:ConvS_00, Cu:ConvS_01 and Cu:HierS_05, while three of them were co-exchanged with both copper and silver; AgCu:ConvS_00, AgCu:ConvS_01 and AgCu:HierS_05.

*Table 4.5: Samples ion-exchanged with the two-step method, the plain SAPO-34 used, and their XRD conclusions.*

| Sample | Plain SAPO-34 | XRD conclusion |
|---|---|---|
| Cu:ConvS_00 | ConvS_00 | CHA |
| Cu:Conv_01 | Conv_01 | CHA |
| Cu:HierS_05 | HierS_05 | CHA |
| AgCu:ConvS_00 | ConvS_00 | CHA |
| AgCu:ConvS_01 | Conv_01 | Not pure phased |
| AgCu:HierS_05 | HierS_05 | CHA |

All the copper ion-exchanged samples made by the two-step method, were crystalline and had CHA topology. The diffractograms of these samples, Cu:ConvS_00, Cu:Conv_01, and Cu:HierS_05, are shown in Figure 4.5

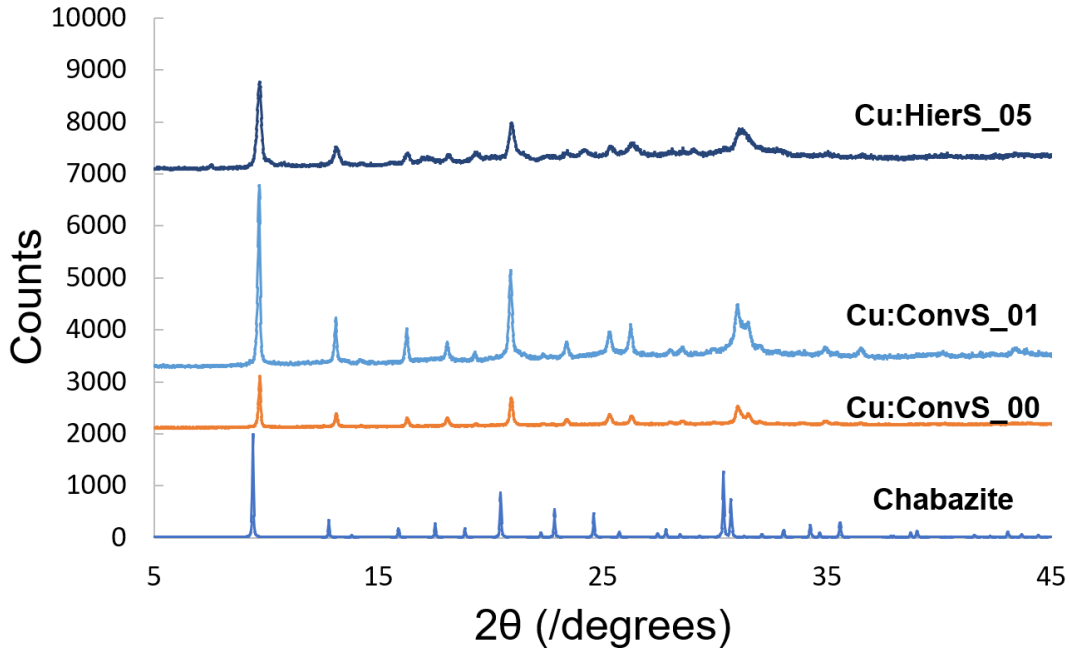


*Figure 4.5: Cu:ConvS_00, Cu:Conv_01 and Cu:HierS_05*

The diffractograms of the three AgCu:SAPO-34 samples are shown in Figure 4.6. Of the AgCu:SAPO-34, two of the samples were crystalline SAPO-34, AgCu:HierS_05 and AgCuConvS_00. The latter sample had about three times lower crystallinity than the first. AgCu:ConvS_01 was not phase pure and had an unknown extra peak.

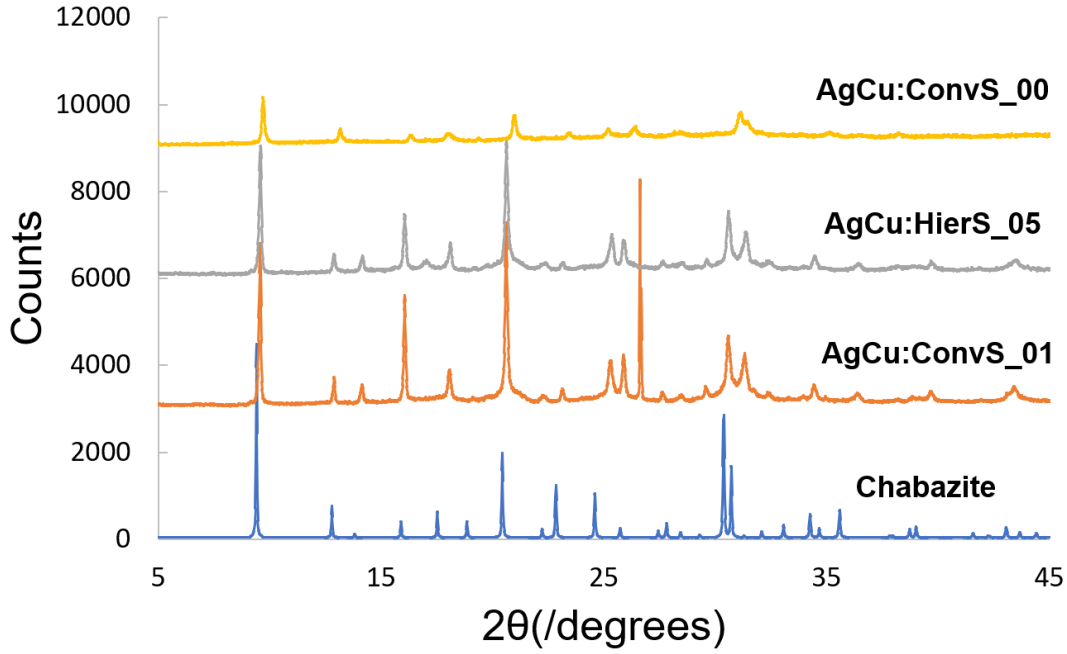


*Figure 4.6: Diffractograms of AgCu:ConvS_00, AgCu:HierS_05, and AgCu:ConvS_01.*

The plain SAPO-34, ConvS_00, was used in the ion-exchange with both the direct method, and the two-step method. The copper ion-exchanged samples made by the two different methods, Cu:ConvS_00D and Cu:ConvS_00, are compared to the calcined ConvS_00 in Figure 4.7. As established, the sample made by the two-step ion-exchange method (Cu:ConvS_00) was crystalline, in contrast to the almost collapsed Cu:ConvS_00D.

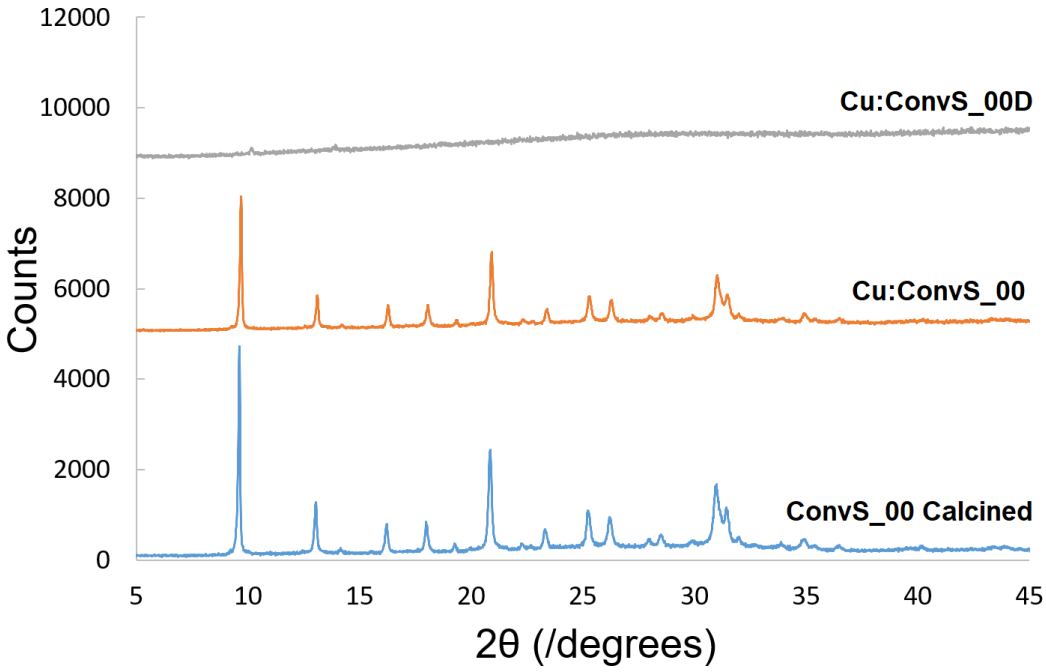


*Figure 4.7: Diffractograms of Cu:ConvS_00D, Cu:CC_00, and ConvS_00 calcined.*

### Overview ion-exchanged SAPO-34

The most important information about all the ion-exchanged samples are gathered in Table 4.6. The table contains information about the original plain SAPO-34 used for the ion-exchange, the methods used, and the XRD results.

*Table 4.6: Overview of the ion-exchanged samples, the original plain SAPO-34, ion-exchange method and the XRD conclusions.*

| Ion-exchanged sample | Plain SAPO | Method | XRD conclusion |
|---|---|---|---|
| Cu:ConvS_00D | ConvS_00 | Direct | Amorph |
| AgCu:ConvS_00D | ConvS_00 | Direct | CHA |
| Cu:ConvS_00 | ConvS_00 | Two-step | CHA |
| AgCu:ConvS_00 | ConvS_00 | Two-step | CHA |
| Cu:HierS_05 | HierS_05 | Two-step | CHA |
| AgCu:HierS_05 | HierS_05 | Two-step | CHA |
| Cu:ConvS_01 | ConvS_01 | Two-step | CHA |
| AgCu:ConvS_01 | ConvS_01 | Two-step | Not pure phased |

### 4.1.3 CuSAPO-34

Three of the samples aiming to be copper incorporated SAPO-34, CuHierS_01, CuHierS_02, and CuHierS_03, are shown in Figure 4.8, and the diffractograms shows that the structures does not match SAPO-34. The diffractogram reveals that none of the structures match SAPO-34. All but one of the seven CuSAPO-34 samples matched the SAPO-20 structure in addition to one peak indicating CuO (not included). The exception was CuHierS_05 that almost collapsed.underwent partial structural collapse.

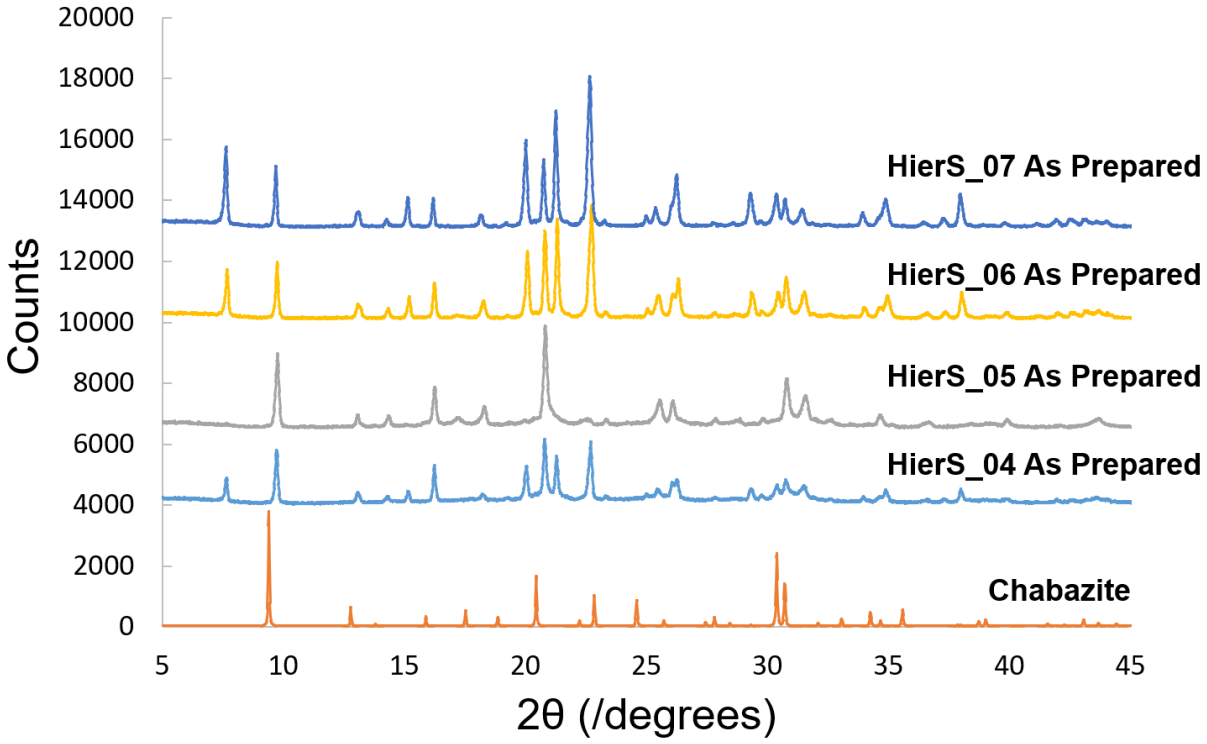


*Figure 4.8: Diffractograms of the copper incorporated SAPO-34 samples CuHierS_01, CuHierS_02, and CuHierS_03.*

## 4.2 BET results

To do the HC-SCR-deNOx, it is important to know that the samples are crystalline which was confirmed with XRD. In this thesis, samples with different porosity are compared, so it is also important to see if the porosity of the samples are different. In addition, the surface areas could be used to compare the different samples. Surface area and pore size distribution measurements, using the BET-BJH method, were conducted on the following phase pure SAPO-34 samples; ConvS_00, ConvS_01 and HierS_05, Cu:ConvS_00, Cu:ConvS_01, Cu:HierS_05, AgCu:ConvS_00D and AgCu:HierS_05.

To establish whether the Cu:HierS_05 was hierarchical, the $N_2$ adsorption-desorption isotherm was compared to the conventional SAPO-34 ConvS_01. The isotherms are given in Figure 4.9. The isotherm for both have a hysteresis loop and looks like the type IV isotherm given by Zeid (2012).[44] The hysteresis loops for ConvS_01 looks like the H4-type given by Zeid (2012).[44] HierS_05 has a slightly larger hysteresis loop than ConvS_01, and looks slightly like a mixture of H4 and H1. HierS_05 seems to adsorb more $N_2$ at higher pressures, that could indicate a more mesoporous structure. No conclusions can be made from this alone since the hysteresis loop can both indicate mesopores and other particles.

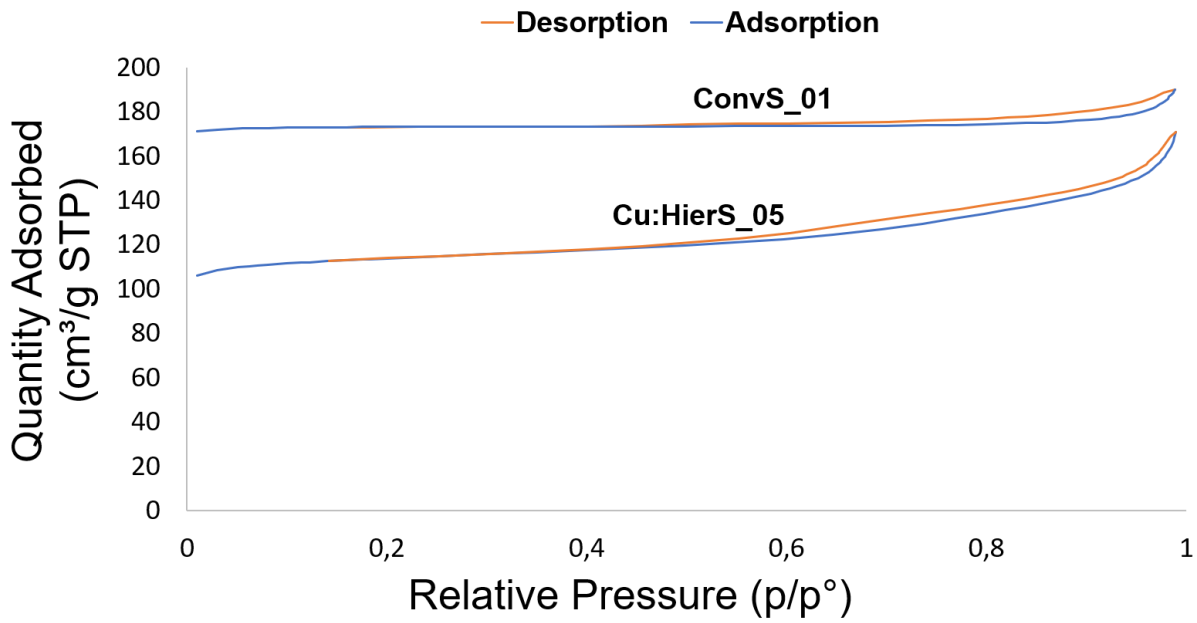


*Figure 4.9: The $N_2$ adsorption/desorption isotherm for ConvS_01 and Cu:HierS_05.*

The pore size distributions of ConvS_01 and Cu:HierS_05 are shown in Figure 4.10; Almost all the pore volume  in ConvS_01 consists of micropores. Cu:HierS_05 have a higher volume of mesopores and have a maxima that indicates mesopores and/or interparticle voids.

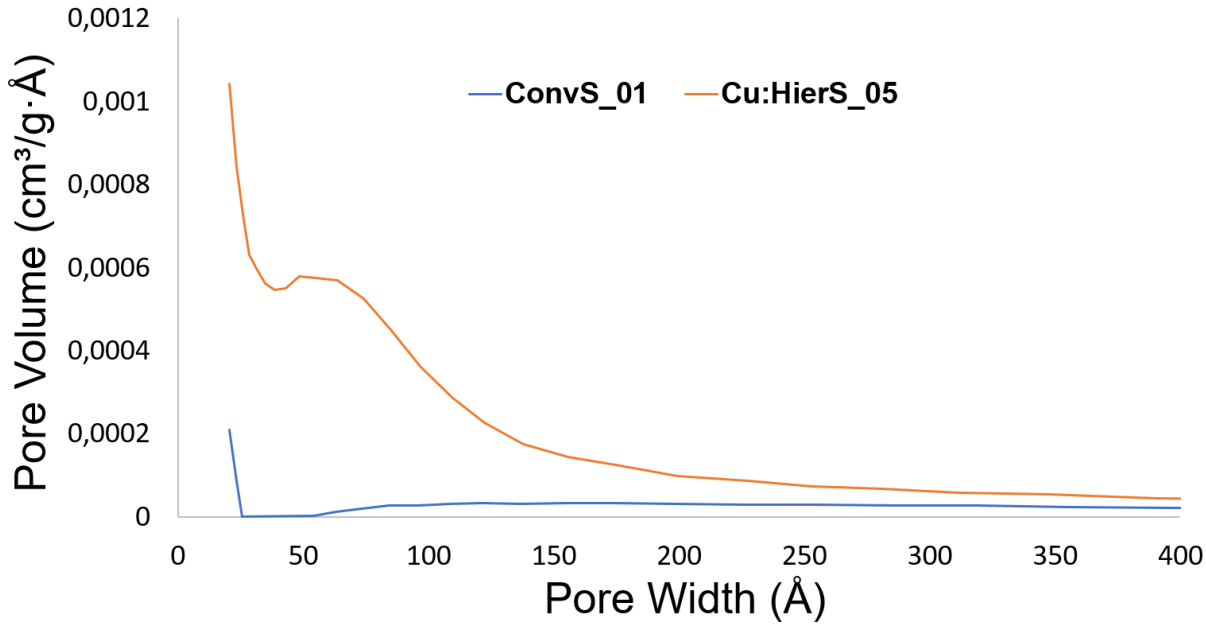


*Figure 4.10: The pore size distribution for the samples ConvS_01 and Cu:HierS_05.*

The specific surface area of the two samples also gives important information and are illustrated in Figure 4.11. This shows that ConvS_01 is conventional as known due to the SDAs added in the synthesis. The BET surface area is 524 m²/g, and 516 m²/g of this is micropore area, which leave almost no external area. Cu:HierS_05 with a BET surface area of 351 $m^2/g$, seems to consist mostly of micropores (301 $m^2/g$), but has an external area of 51 m²/g. Also, the pore size distribution showed the presence of mesopores, so the material is probably hierarchical.

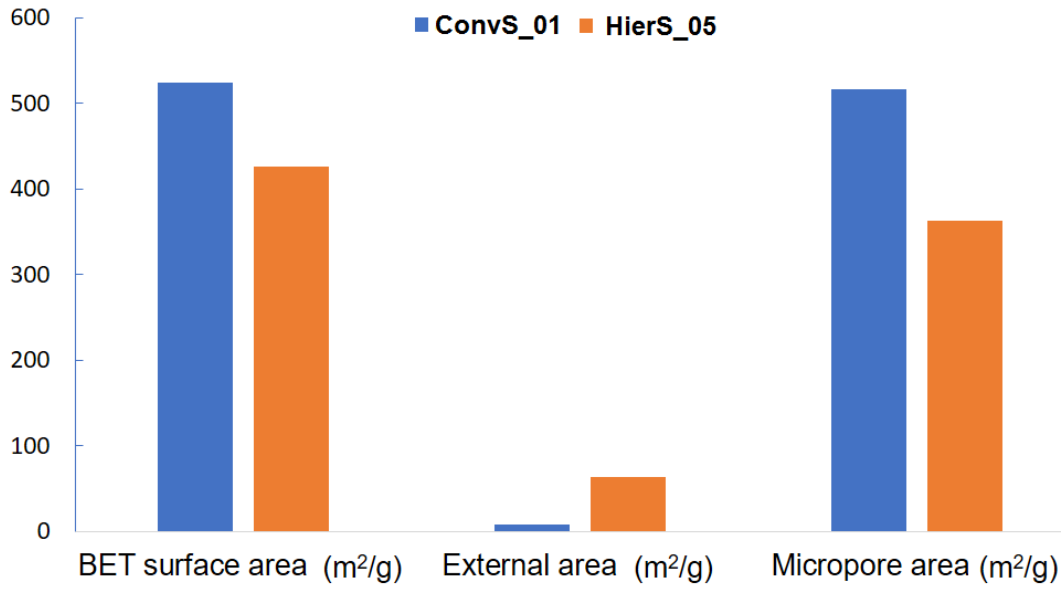


*Figure 4.11: Surface area, external area and micropore area for the samples ConvS_01 and Cu:HierS_05.*

The isotherm linear plots of all the samples used in the HC-SCR-deNOx are showed in Figure 4.12. The conventional samples seemed to have an isotherm type IV, with H4-type hysteresis loops, the hysteresis loops indicating the material only consists of micropores. The conventional samples, both HierS_05 and Cu:HierS_05 seems to adsorb more $N_2$ at higher pressures, indicating additional mesopores or other particles.

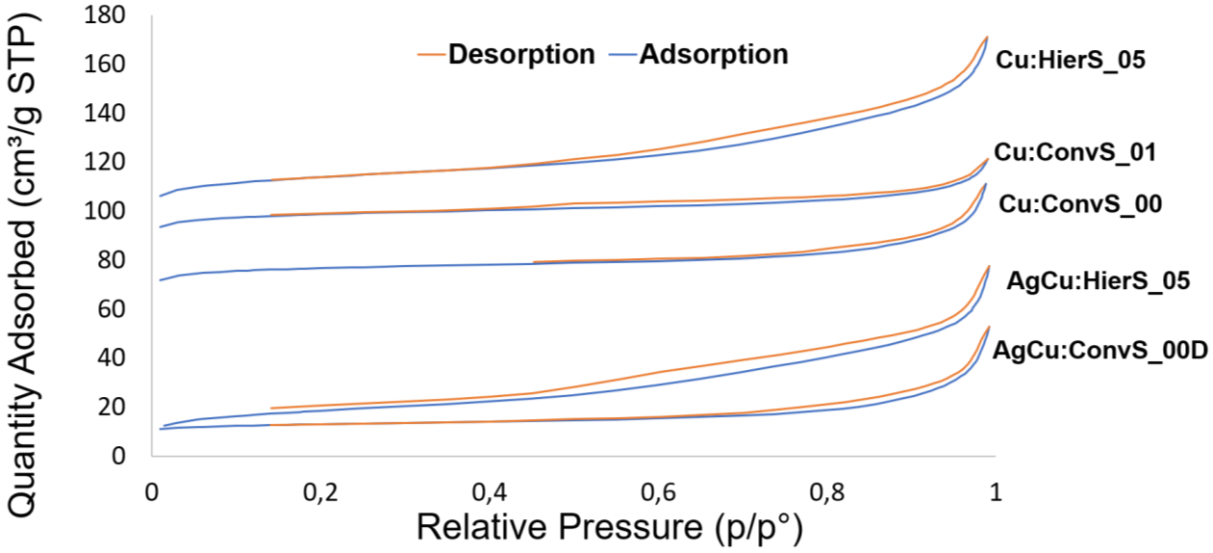


*Figure 4.12: Linear isotherm plots of Cu:HierS_05, Cu:ConvS_01, Cu:ConvS_00, AgCu:HierS_05 and AgCu:ConvS_00.*

All of the ion-exchanged samples had a reduced surface area compared to their respective plain SAPOs, except for the ones made with HierS_05. The BET specific surface area, external area and micropore area for all the samples are shown in Table 4.7. HierS_05 has a much lower BET surface area, 179 $m^2/g$, than the copper ion-exchanged sample Cu:HierS_05, 352 $m^2/g$. The surface area of the rest of the plain SAPO-34 samples are shown in the appendix.

*Table 4.7: The BET specific surface area, external area and micropore area of the mother SAPO-34 samples and ion-exchanged SAPO-34 samples.*

| **Sample name** | **BET surface area ($m^2/g$)** | **External area ($m^2/g$)** | **Micropore area ($m^2/g$)** |
|---|---|---|---|
| ConvS_00 | 480 | 35 | 446 |
| Cu:ConvS_00 | 235 | 26 | 209 |
| ConvS_01 | 524 | 8 | 516 |
| Cu:ConvS_01 | 302 | 28 | 274 |
| HierS_05 | 179 | 49 | 130 |
| Cu:HierS_05 | 352 | 51 | 301 |
| AgCu:ConvS_00D | 41 | 15 | 27 |
| AgCu:HierS_05 | 63 | 48 | 15 |

The surface area, micropore area and external area of the successful ion-exchanged samples are shown in Figure 4.13. Both of the AgCu:SAPO-34 had a much lower BET-surface (41 $m^2/g$ - 63 $m^2$) than the Cu:SAPO-34 (235 $m^2/g$ - 352 $m^2/g$).

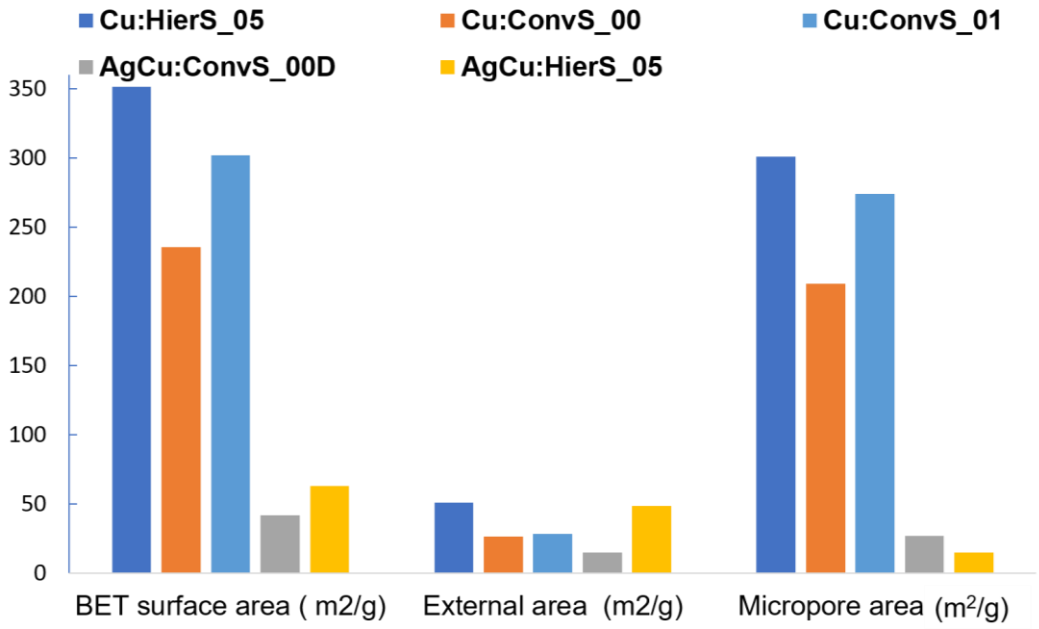


*Figure 4.13: The surface area, micropore area and external area of the ion-exchanged samples.*

Since the Ag:SAPO-34 had such low BET specific surface area compared to the Cu:SAPO-34 samples, the pore size distribution of the pores in sample Cu:HierS_05 and AgCu:HierS_05 were compared, showed in Figure 4.14. It shows that the mean pore size for AgCu:HierS_05 is a bit smaller than for Cu:HierS_05, and both have a mean pore size with a pore width larger than for micropores.

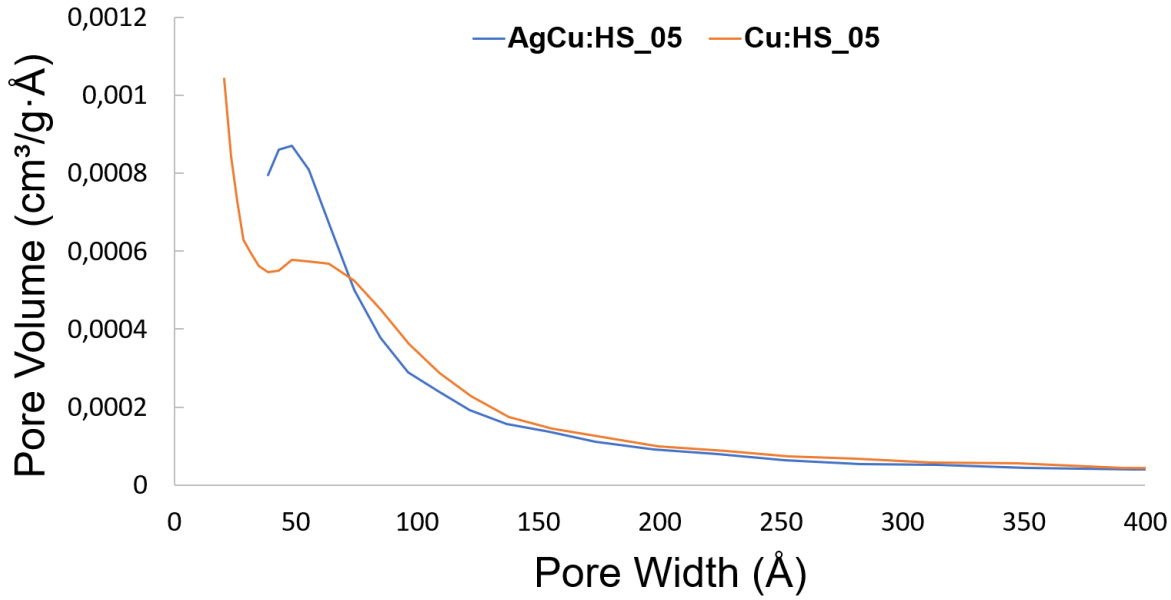


*Figure 4.14: Pore size distribution for the samples Cu:HierS_05 and AgCu:HierS_05.*

### 4.3 ICP-MS results

The results of the elemental ICP-MS analysis are shown in Figure 4.15: The AgCu:ConvS_00D contains 2.8 wt% copper and 2.9 wt% silver, which is about three times more of both copper and silver than AgCu:HierS_05 which contains 0.9 wt% copper and 0.7 wt% silver. For the Cu:SAPO-34 samples, the copper content varies from 2.3 wt% to 3.1 wt%, and Cu:ConvS_01 has the highest copper content, 3.1 wt%. Of the Cu:SAPO-34 samples, Cu:ConvS_00 has the lowest content of copper, 2.3 wt%, followed by Cu:HierS_05 with 2.5 wt% of copper.

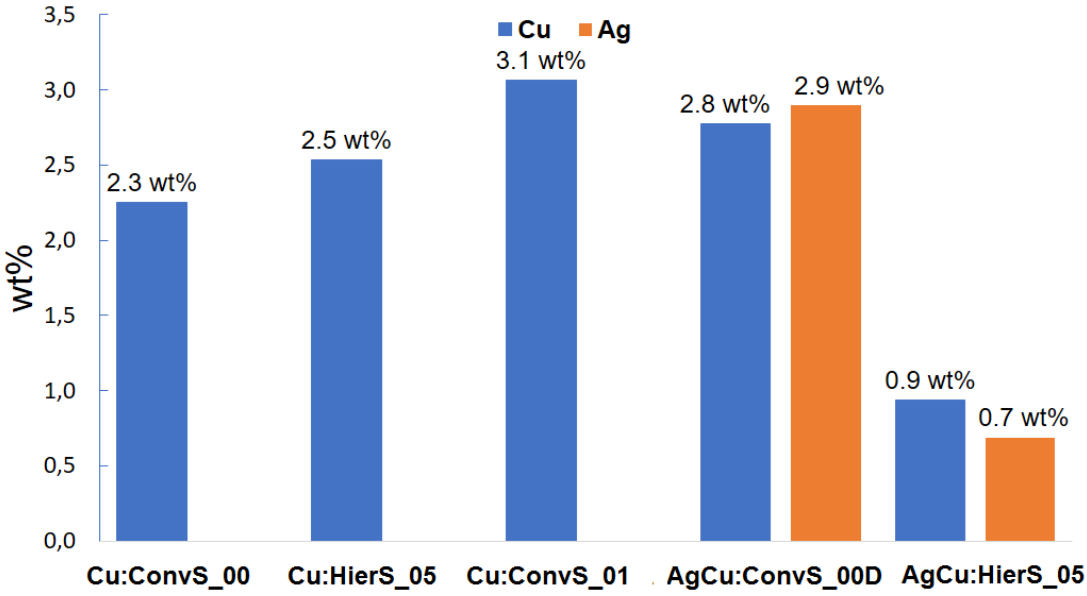


*Figure 4.15: ICP-MS results for Cu:ConvS_00, Cu:HierS_05, Cu:ConvS_01, AgCu:ConvS_00D and AgCu:HierS_05, showing the content of copper and silver in each sample.*

## 4.4 HC-SCR-deNOx catalytic measurements

In this section, the deNOx results for the Cu:SAPO-34 and AgCu:SAPO-34 samples are compared. Three of the samples used in the catalysis were in dry feed (Cu:ConvS_00, AgCu:HierS_05, AgCu:ConvS_00D), and two of them were in wet feed (Cu:HierS_05, Cu:ConvS_01). The samples are listed in Table 4.8, which also contains BET surface area, metal content and if the sample was in a dry or wet feed.

*Table 4.8: BET surface area, metal content and wet/dry feed for the samples used in the HC-SCR-deNOx.*

| | **BET surface area ($m^2/g$)** | **Cu (wt%)** | **Ag (wt%)** | **Feed** |
|---|---|---|---|---|
| **Cu:ConvS_00** | 235 | 2.3 | – | Dry feed |
| **Cu:ConvS_01** | 302 | 3.1 | – | Wet feed |
| **Cu:HierS_05** | 352 | 2.5 | – | Wet feed |
| **AgCu:ConvS_00D** | 42 | 2.8 | 2.9 | Dry feed |
| **AgCu:HierS_05** | 63 | 0.9 | 0.7 | Dry feed |

Figure 4.16 shows the NOx conversion for the copper ion-exchanged SAPO-34 in dry feed (Cu:ConvS_01 and Cu:HierS_05) and wet feed (Cu:ConvS_00). The samples in the wet feed, Cu:HierS_05 and Cu:ConvS_01 had respectively 58.3% and 59.2% conversions, which were lower conversions than for the sample in dry feed, Cu:ConvS_00, with 70% conversion. Cu:ConvS_00 reached over 60% conversion that is quite steady from about 325°C to 500°C. In the wet feed, the hierarchical sample (Cu:HierS_05) had lower conversion than Cu:ConvS_01 in the temperatures below 400°C, but show higher NOx conversion above 400°C

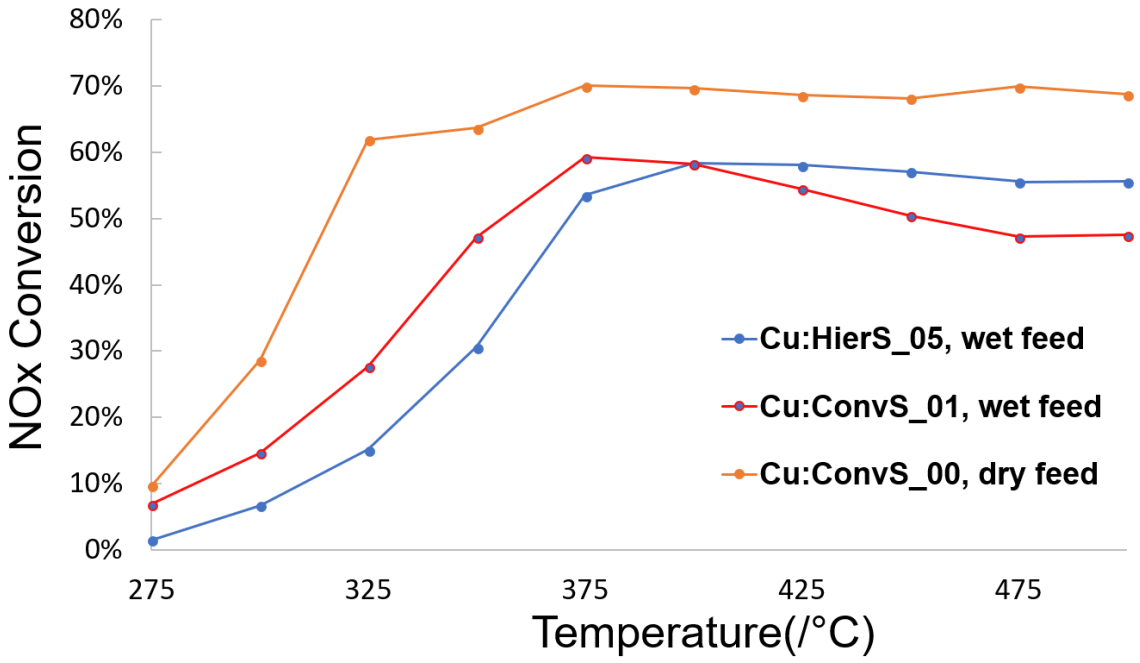


*Figure 4.16: NOx conversion of the copper ion-exchanged samples in both wet and dry feed, Cu:ConvS_00, Cu:HierS_05 and Cu:ConvS_01. The orange line represents dry feed, the blue line represents wet feed.*

For the AgCu:SAPO-34 samples, the conversion was a bit lower than for Cu:SAPO-34, see Figure 4.17. AgCu:ConvS_00D had 16.1% as the highest reached conversion reached, while AgCu:HierS_05 had higher conversion, 54.2%. Both samples had a dry feed during the deNOx.

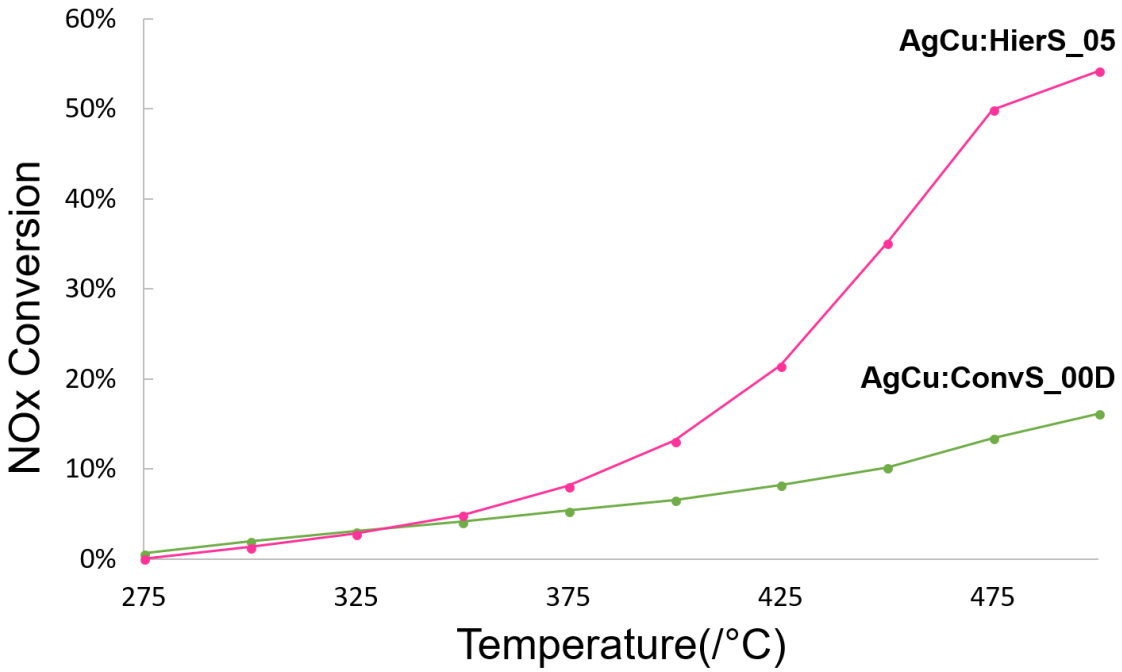


*Figure 4.17: Conversion of NOx for both AgCu:ConvS_00 and AgCu:HierS_05. Both in dry feed.*

The highest conversion of all the samples are given in Figure 4.18. The highest convention achieved was 70% by Cu:ConvS_00, and the Cu:SAPO-34 samples all had higher conversion than the ones also containing silver, also including experiments performed in wet feed.

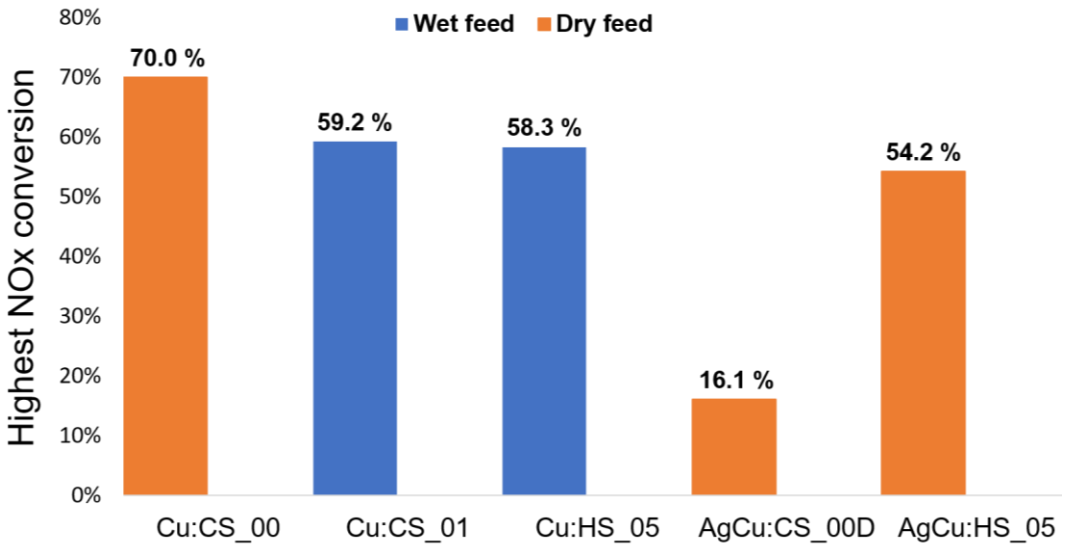


*Figure 4.18: Highest reached conversion for each sample, both for wet and dry feed. The blue bars represent wet feed, the orange bars represent dry feed.*

The activity of the samples used in the catalysis, is shown in Table 4.9. The sample are in this thesis considered active if the conversion is 30% or above. The capital M indicates the temperature the highest convention was achieved. Cu:ConvS_00 is active over the longest temperature range (325°C-500°C), while AgCu:HierS_05 is considered inactive. Cu:ConvS_01 and HierS_05 are both active over the same temperature range, 350°C - 500°C. Both of the AgCu:SAPO-34 had their highest conversion at 500 °C. For the Cu:SAPO-34 samples, Cu:ConvS_00 and Cu:ConvS_01 both had their highest conversion at 375 °C, and Cu:HierS_05 had its highest conversion at 400°C.

*Table 4.9: Overview of the temperature range for deNOx-active SAPO-34 samples*

| **Temperature (/°C)** | **275** | **300** | **325** | **350** | **375** | **400** | **425** | **450** | **475** | **500** |
|---|---|---|---|---|---|---|---|---|---|---|
| **Cu:ConvS_00** | | | | | M | | | | | |
| **Cu:ConvS_01** | | | | | M | | | | | |
| **Cu:HierS_05** | | | | | | M | | | | |
| **AgCu:ConvS_00D** | | | | | | | | | | M |
| **AgCu:HierS_05** | | | | | | | | | | M |

'M' marks the temperature for maximum conversion of the listed samples.

# 5.0 Discussion

The main goal for this thesis, was to investigate the catalytic performance in the HC-SCR-de$NO_x$ reaction for both hierarchical and conventional SAPO-34 containing AgCu and Cu species. To introduce copper and silver ions into SAPO-34, different methods were tried. This thesis was a continuation of another thesis written by Botne (2017)[1], which enlightened a known issue with structural collapse of SAPO-34 due to irreversible hydrolysis of Cu:SAPO-34 during the ion-exchange process. An important part of this study was therefore to find a solution to do the ion-exchange and avoid structural collapse of the SAPO-34 structure. Important information about the samples are gathered in Table 5.1. This includes information about the BET surface area, external area, micropore area, copper and/or silver content, and the highest conversion reached of the samples. The rows in blue indicates that the NOx HC-SCR was done in a wet feed, the white rows indicates catalytic measurements performed in a dry feed.

*Table 5.1: BET specific surface area, external area, micropore area, copper and/or silver content, and the highest NOx conversion reached for each sample. The blue colour indicates that the deNOx conversion was done in a wet feed, the white indicates a dry feed.*

| | **BET surface area ($m^2/g$)** | **External Area ($m^2/g$)** | **Micropore area ($m^2/g$)** | **Cu (wt%)** | **Ag (wt%)** | **Highest conversion (%)** |
|---|---|---|---|---|---|---|
| Cu:ConvS_00 | 235 | 26 | 209 | 2.3 | – | 70 |
| Cu:ConvS_01 | 302 | 28 | 274 | 3.1 | – | 59.3 |
| Cu:HierS_05 | 352 | 51 | 301 | 2.5 | – | 58.3 |
| AgCu:ConvS_00D | 42 | 15 | 26 | 2.8 | 2.9 | 16.1 |
| AgCu:HierS_05 | 63 | 48 | 15 | 0.9 | 0.7 | 54.2 |

The ion-exchange was carried out using two different approaches; Direct ion-exchange and two-step ion-exchange. For Cu:SAPO-34, the same plain SAPO-34, ConvS_00, was ion-exchanged using both approaches. The sample directly ion-exchanged with copper (Cu:ConvS_00D) almost collapsed, just like the similar sample made by Botne (2017).[1] The sample made by the two-step ion-exchange (Cu:ConvS_00) exhibited a specific surface area

of 235 $m^2/g$ and was crystalline. This indicates that the two-step method prevented the irreversible hydrolysis as described by Xu. Et.al (2017).[2]

The Cu:SAPO-34 and AgCu:SAPO-34 samples, confirmed to be phase pure by XRD, were tested for the HC-SCR-deNOx reaction. Comparing this sample and the other samples in dry feed, the water in the reaction gas feed does not appear to have a substantial effect on the NOx conversion (table 5.1). Both samples in the wet feed, Cu:ConvS_01 and Cu:HierS_05, obtained its highest conversion about 10 percentage points lower than the sample with the overall highest achieved conversion, Cu:ConvS_00. This is as could be expected according to the research of Ishihara et. al (1997).[48] Their sample in a dry feed had an 80% conversion of NOx at 300°C, and in wet feed (15 vol. % water) they report a conversion just below 70% at about 325°C.

For the Cu:SAPO-34, the highest reached conversion between the hierarchical and conventional samples in the wet feed were respectively 59.2% versus 58.3%, which is quite similar. Even though the highest conversion was similar, the conversion above 400°C of Cu:HierS_05 was about 10% better than Cu:ConvS_01. Cu:ConvS_01 had about 10% higher conversions below 400°C. The diffusion limits in the conventional SAPO-34, and the mesopores in hierarchical materials that should work as "highways", could contribute to higher conversions of the hierarchical SAPO-34, but in this study, their conventions were similar.[49] Diffusion limitations could also result in propene poisoning, causing deactivation of Cu-SSZ-13 (a chabazite zeolite) due to coke deposition and pore blockage at medium temperature ranges ( approximately around 350°C).[50] Supports that the results, that the conversion of the hierarchical samples had the highest activity above medium temperature, here above 400°C for the Cu:SAPO-34, and above 350°C for AgCu:SAPO-34.

The AgCu:SAPO-34 samples were run in a dry feed and did not have as high conversion as the samples only containing copper. One of them, AgCu:HierS_05, had only a few percent lower than the Cu:SAPO-34 samples in wet feed, 54.2% at 500°C. This is a high conversion compared to the similar sample made by Botne (2017)[1], which had about 15% conversion at 500°C [1]. Figure 5.1 shows the conversions done in this thesis (blue bars), compared to the similar samples made by Botne (green bars). A difference to take note to, is that Botne's sample with the highest reached conversion, the conventional AgCu:SAPO-34 with 83% conversion, had an even higher metal content than all the samples tested in this thesis. There

is therefore no detected correlation between high conversion and high copper and/or silver content, see Figure 5.1 for the copper and/or silver content in the rest of the samples. Surprisingly the other co-exchanged sample in this thesis, AgCu:ConvS_00D, had a maximum conversion at only 16.1%. Especially, this is interesting since AgCu:ConvS_00D is made from the same plain SAPO-34 as Cu:ConvS_00, which had the highest conversion of all the samples. Zuo et.al (2013) found that high surface area can lead to higher catalytic activity[51], which could explain the low activity of AgCu:ConvS_00D. AgCu:ConvS_00D had a low BET surface area, 42 $m^2/g$, which is very small compared to Cu:ConvS_00, exhibiting 235 $m^2/g$. The conversion is almost the same as for Botne's (2017) co-exchanged sample, thus his sample is hierarchical.

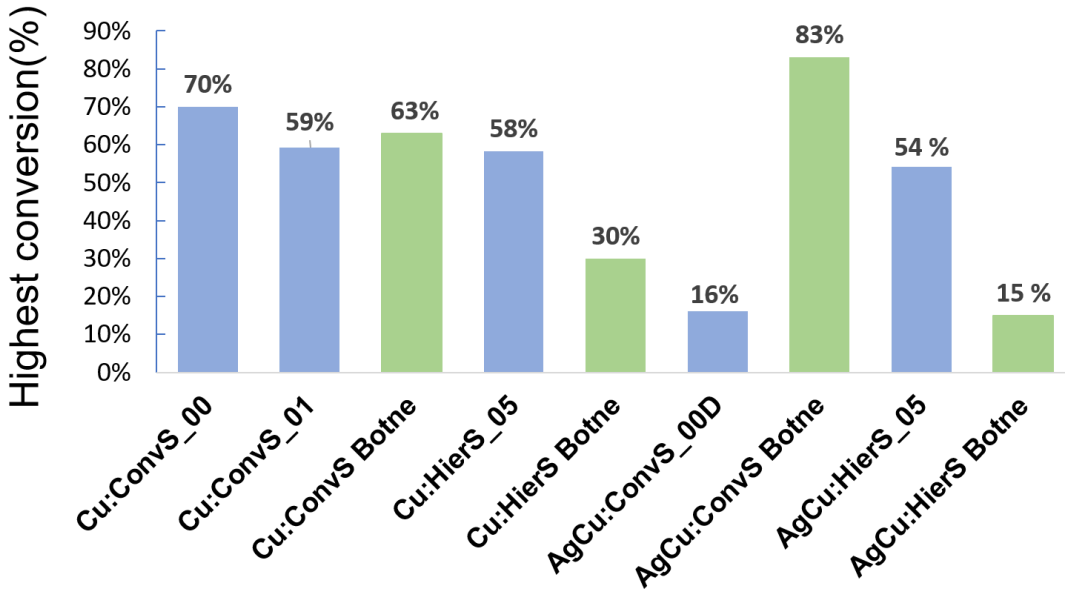


*Figure 5.1: Highest reached NOx conversion of the samples used in deNOx in this thesis, and the similar samples made by Botne (2017)[1].*

AgCu:ConvS_00D had the lowest external surface area of all of the samples, 15 $m^2/g$, and also the lowest conversion (16%). The study of Zheng et. al (2016) reported that the low external surface area indicates large particles.[52] The surface area of the samples containing silver significantly lower (42-63 $m^2/g$) than the one only containing copper (235-352 $m^2/g$), indicating pore blockage in the SAPO-34 samples containing silver, possibly due to formation of Ag particles.[55]

A possible explanation for the poor catalytic performance of the AgCu:ConvS_00D could as mentioned be explained by the low specific surface area at 42 $m^2/g$, but AgCu:HierS_05 had a highest reached conversion of 54.2% even though the BET specific surface area also was low, 63 $m^2/g$. The sample changed colour from light blue to grey after dehydration, so a possible explanation could be that the silver was reduced, and this could cause silver particles to block the pores, and exclude the internal area from the results.[55] This fits the results of the pore size distribution results from the BJH.[53] The AgCu:SAPO-34 samples used in BET/BJH was not reused for the HC-SCR-deNOx.

The NOx conversions of the samples used in this thesis is compared to similar samples from Botne's thesis, in Table 5.2. The capital M indicates the temperature at which the highest convention was achieved. The co-exchanged SAPO-34 with silver and copper in this thesis, both had their highest conversion at 500°C, versus 375°C and 400°C for the copper containing samples.

Table 5.2: Activity temperature range for all the samples used in the catalysis. Capital M indicates highest conversion reached.

| **Temperature (/°C)** | **275** | **300** | **325** | **350** | **375** | **400** | **425** | **450** | **475** | **500** |
|---|---|---|---|---|---|---|---|---|---|---|
| **Cu:ConvS_00** | | | | | M | | | | | |
| **Cu:ConvS_01** | | | | | M | | | | | |
| **Cu:ConvS Botne** | | | | | | | | | M | |
| **Cu:HierS_05** | | | | | | M | | | | |
| **Cu:HierS Botne** | | | | | | M | | | | |
| **AgCu:ConvS_00D** | | | | | | | | | | M |
| **AgCu:ConvS Botne** | | | | | | | M | | | |
| **AgCu:HierS_05** | | | | | | | | | | M |
| **AgCu:HierS Botne** | | | | | | | | | M | |

The hierarchical samples Cu:HierS_05 and AgCu:HierS_05 had high temperature activity range (350°C - 500°C and 450°C -500°C) compared to the hierarchical samples made by Botne (2017)[1] (400°C, and not active at any temperature), as seen in Table 5.2. All of the samples were active in a broader temperature range than Botne's similar samples, except for AgCu:ConvS_00D. It seems to be a correlation between the broad temperature activity range and a high conversion of the samples. Comparing similar samples, the only samples not following this correlation were the conventional Cu:SAPO-34. Since the experimental conditions were not the same (Botne's sample were in a dry feed, Cu:ConvS_00 and Cu:ConvS_01 were in a wet feed) they can't be directly compared.

# 6.0 Conclusion

The hierarchical SAPO-34 with incorporated copper was not successfully synthesized, and the direct ion-exchange of SAPO-34 with copper was not successful either; It almost collapsed and was amorph. However, conventional and hierarchical SAPO-34 was synthesized and successfully ion-exchanged with copper and with silver in a two-step method. The co-exchange with copper and silver was successful with both methods.

For the AgCu:SAPO-34 directly ion-exchanged, the surface area was smaller than the similar sample ion-exchanged in two steps, which was also reflected in the conversion which were much higher for the sample ion-exchanged in two steps. The Cu:SAPO-34 directly ion-exchange could not be used for the deNOx. All but one of the samples were active during NOx conversion in HC-SCR. The presence of mesopores in the hierarchical Cu:SAPO-34 did not seem to influence conversion in this study. For the co-exchanged AgCu:SAPO-34, the hierarchical sample had the highest conversion. High surface area did seem to equal higher conversion in the dry feed, but in the wet feed the surface area did not correspond to the conversion. The presence of water in the feed did not reduce the NOx conversion remarkable, about 10 percentage points. Compared to the results in Botne's (2017)[1] thesis, the conversion of the conventional AgCu:SAPO-34 was really low, and the hierarchical AgCu:SAPO-34 high. The rest of the highest conversion reached by the samples in the two theses were quite similar, but most of them showed a higher activity range at a lower temperature in this study. Also, there was not found any obvious correspondence between metal content and catalytic activity when the samples were compared to the results reported by Botne, but it seems to be a correlation between activity in a broad temperature range and a high conversion of the samples.

# 7.0 Further work

For further work the samples tested in dry feed (Cu:ConvS_00, AgCu:ConvS_00D and AgCu:HierS_05) should be tested in a wet feed, and visa versa with the samples tested in wet feed (Cu:ConvS_01 and Cu:HierS_05), to better see the effect of hydrothermal stability. The HierS_05 and Cu:HierS_05 should be investigated to figure out why the BET specific surface area increased after the ion-exchange. The crystalline sample AgCu:ConvS_00 was not tested due to technical problems and should be tested in both dry and wet feed. Also, different hydrocarbons than propene could be tested, etc. methane or isobutene, to test the effect of using different size reductants. Due to the difference in conversions of the two AgCu:SAPO-34, a good idea could be to investigate the position of metal atoms after ion-exchange. In addition to this, the method to incorporate copper into the framework of SAPO-34 should be analysed further, by for example alternate different synthesis parameters and using different templates.

# 8.0 References


1. Botne, G. The effect of mechanical mixing and porosity on the activity of Ag and Cu ion exchanged zeotypes in the HC-SCR of NOx with propene. NTNU, Trondheim, 2017.
2. Xu, M.; Wang, J.; Wang, J.; Shen, M.; Yu, T., *New insight into Cu/SAPO-34 preparation procedure: Impact of NH 4 -SAPO-34 on the structure and Cu distribution in Cu-SAPO-34 NH 3 -SCR catalysts*. 2017; Vol. 220.
3. Sharma, N.; Agarwal, A. K.; Eastwood, P.; Gupta, T.; Singh, A. P., Introduction to Air Pollution and Its Control. In *Air Pollution and Control*, Sharma, N.; Agarwal, A. K.; Eastwood, P.; Gupta, T.; Singh, A. P., Eds. Springer Singapore: Singapore, 2018; pp 3-7.
4. Faiz, A.; Weaver, C. S.; Walsh, M. P., *Air Pollution from Motor Vehicles: Standards and Technologies for Controlling Emissions*. World Bank: 1996.
5. Dorado, M. P.; Ballesteros, E.; Arnal, J. M.; Gómez, J.; López, F. J., Exhaust emissions from a Diesel engine fueled with transesterified waste olive oil☆. *Fuel* **2003,** *82* (11), 1311-1315.
6. (EPA), E. P. A. Effects of Acid Rain. https://www.epa.gov/acidrain/effects-acid-rain (accessed 14.05).
7. Miljødirektoratet Nitrogenoksid(NOx). http://www.miljostatus.no/Tema/Luftforurensning/Sur-nedbor/Nitrogenoksid-NOx (accessed 27.05.18).
8. Miljødirektoratet Kyotoprotokollen. http://www.miljostatus.no/tema/klima/internasjonal-klimapolitikk/kyotoprotokollen/ (accessed 01.05).
9. Hotten, R. Volkswagen: The scandal explained. http://www.bbc.com/news/business-34324772 (accessed 12.05).
10. Mrad, R.; Aissat, A.; Cousin, R.; Courcot, D.; Siffert, S., Catalysts for NOx selective catalytic reduction by hydrocarbons (HC-SCR). *Applied Catalysis A: General* **2015,** *504*, 542-548.
11. Weisweiler, W.; Hizbullah, K.; Kureti, S., Simultaneous Catalytic Conversion of NOx and Soot from Diesel Engines Exhaust into Nitrogen and Carbon Dioxide. *Chemical Engineering & Technology* **2002,** *25* (2), 140-143.
12. Lee, K.; Ogita, Y.; Sato, S.; Kosaka, H., *NOx Reduction with the HC-SCR System over Cu/Zeolite Based Catalysts*. 2015.

13. Rao, G. R.; Mishra, G. B., *Structural, Redox and Catalytic Chemistry of Ceria Based Materials*. 2003; Vol. 2.

14. Holma, T.; Palmqvist, A.; Skoglundh, M.; Jobson, E., Continuous lean NOx reduction with hydrocarbons over dual pore system catalysts. *Applied Catalysis B: Environmental* **2004,** *48* (2), 95-100.

15. Savva, P. G.; Costa, C. N., Hydrogen Lean-DeNOx as an Alternative to the Ammonia and Hydrocarbon Selective Catalytic Reduction (SCR). *Catalysis Reviews* **2011,** *53* (2), 91-151.

16. Anderson, J. A.; García, M. F., *Supported Metals in Catalysis*. Imperial College Press: London, 2005; Vol. 5, p 285-292.

17. Miyazaki, K.; Eskes, H.; Sudo, K.; Boersma, K. F.; Bowman, K.; Kanaya, Y., Decadal changes in global surface NOx emissions from multi-constituent satellite data assimilation. *Atmos. Chem. Phys.* **2017,** *17* (2), 807-837.

18. Sector share of nitrogen oxides emissions. https://www.eea.europa.eu/data-and-maps/daviz/sector-share-of-nitrogen-oxides-emissions#tab-chart_1 (accessed 14.05).

19. Speight, J. G., Chapter 4 - Sources and Types of Organic Pollutants. In *Environmental Organic Chemistry for Engineers*, Butterworth-Heinemann: 2017; pp 153-201.

20. Holgate, S. T.; Thomas, M., Chapter 7 - Asthma. In *Middleton's Allergy Essentials*, Elsevier: 2017; pp 151-204.

21. Hagen, J., *Industrial Catalysis: A Practical Approach*. Third completely revised and enlarged edition. ed.; Germany: Wiley-VCH: 2015.

22. Lok, B. M.; Messina, C. A.; Patton, R. L.; Gajek, R. T.; Cannan, T. R.; Flanigen, E. M., Silicoaluminophosphate molecular sieves: another new class of microporous crystalline inorganic solids. *Journal of the American Chemical Society* **1984,** *106* (20), 6092-6093.

23. Djieugoue, M.-A.; Prakash, A. M.; Kevan, L., Electron Spin Resonance and Electron Spin Echo Modulation Studies on Reducibility, Location, and Adsorbate Interactions of Ni(I) in Ni(II)-Exchanged SAPO-34. *The Journal of Physical Chemistry B* **1998,** *102* (22), 4386-4391.

24. Cundy, C. S.; Cox, P. A., The Hydrothermal Synthesis of Zeolites: History and Development from the Earliest Days to the Present Time. *Chemical Reviews* **2003,** *103* (3), 663-702.

25. Auerbach, S. M.; Carrado, K. A.; Dutta, P. K., *Handbook of zeolite science and technology*. Marcel Dekker: New York, 2003.

26. Vajtai, R., Springer Handbook of Nanomaterials. Vajtai, R., Ed. Springer Berlin Heidelberg : Imprint: Springer: 2013.

27. Hartmann, M.; Kevan, L., Transition-Metal Ions in Aluminophosphate and Silicoaluminophosphate Molecular Sieves: Location, Interaction with Adsorbates and Catalytic Properties. *Chemical Reviews* **1999,** *99* (3), 635-664.

28. Salmasi, M.; Fatemi, S.; Hashemi, S. J., MTO reaction over SAPO-34 catalysts synthesized by combination of TEAOH and morpholine templates and different silica sources. *Scientia Iranica* **2012,** *19* (6), 1632-1637.

29. Database of Zeolite Structures. http://europe.iza-structure.org/IZA-SC/framework.php?STC=CHA (accessed 01.05).

30. Anderson, M. W.; Sulikowski, B.; Barrie, P. J.; Klinowski, J., In situ solid-state NMR studies of the catalytic conversion of methanol on the molecular sieve SAPO-34. *The Journal of Physical Chemistry* **1990,** *94* (7), 2730-2734.

31. Venna, S. R. C., Moises A., Microwave assisted phase transformation of silicoaluminophosphate zeolite crystals. *Journal of Materials Chemistry* **2009,** (48), 3138-3140.

32. Jhung, S. H.; Chang, J.-S.; Hwang, J. S.; Park, S.-E., Selective formation of SAPO-5 and SAPO-34 molecular sieves with microwave irradiation and hydrothermal heating. *Microporous and Mesoporous Materials* **2003,** *64* (1), 33-39.

33. Valizadeh, B.; Askari, S.; Halladj, R.; Haghmoradi, A., Effect of Synthesis Conditions on Selective Formation of SAPO-5 and SAPO-34. *Synthesis and Reactivity in Inorganic, Metal-Organic, and Nano-Metal Chemistry* **2014,** *44* (1), 79-83.

34. Li, S.; Falconer, J. L.; Noble, R. D., SAPO-34 membranes for CO2/CH4 separations: Effect of Si/Al ratio. *Microporous and Mesoporous Materials* **2008,** *110* (2), 310-317.

35. Feliczak-Guzik, A., Hierarchical zeolites: Synthesis and catalytic properties. *Microporous and Mesoporous Materials* **2018,** *259*, 33-45.

36. Miletto, I.; Ivaldi, C.; Paul, G.; Chapman, S.; Marchese, L.; Raja, R.; Gianotti, E., Hierarchical SAPO-34 Architectures with Tailored Acid Sites using Sustainable Sugar Templates. *ChemistryOpen* **2018,** *7* (4), 297-301.

37. Perez-Ramirez, J.; Christensen, C. H.; Egeblad, K.; Christensen, C. H.; Groen, J. C., Hierarchical zeolites: enhanced utilisation of microporous crystals in catalysis by advances in materials design. *Chemical Society Reviews* **2008,** *37* (11), 2530-2542.

38. Gao, F.; Walter, E. D.; Washton, N. M.; Szanyi, J.; Peden, C. H. F., Synthesis and Evaluation of Cu-SAPO-34 Catalysts for Ammonia Selective Catalytic Reduction. 1. Aqueous Solution Ion Exchange. *ACS Catalysis* **2013,** *3* (9), 2083-2093.

39. Xiang, X.; Cao, Y.; Sun, L.; Wu, P.; Cao, L.; Xu, S.; Tian, P.; Liu, Z., Improving the low-temperature hydrothermal stability of Cu-SAPO-34 by the addition of Ag for ammonia selective catalytic reduction of NOx. *Applied Catalysis A: General* **2018,** *551*, 79-87.

40. Burrington, J. D., *Industrial catalysis : chemistry and mechanism*. Imperial College Press: London, 2016; p 238-245.

41. Poole, C. P., *Introduction to nanotechnology*. Wiley-Interscience: Hoboken, N.J, 2003.

42. Skalny, J.; Hearn, N., 13 - Surface Area Measurements. In *Handbook of Analytical Techniques in Concrete Science and Technology*, William Andrew Publishing: Norwich, NY, 2001; pp 505-527.

43. Berk, Z., Chapter 12 - Adsorption and Ion Exchange. In *Food Process Engineering and Technology (Second Edition)*, Academic Press: San Diego, 2013; pp 311-327.

44. Alothman, Z., *A Review: Fundamental Aspects of Silicate Mesoporous Materials*. 2012; Vol. 5, p 2874-2902.

45. Villarroel-Rocha, J.; Barrera, D.; Sapag, K., Introducing a self-consistent test and the corresponding modification in the Barrett, Joyner and Halenda method for pore-size determination. *Microporous and Mesoporous Materials* **2014,** *200*, 68-78.

46. Barrett, E. P.; Joyner, L. G.; Halenda, P. P., The Determination of Pore Volume and Area Distributions in Porous Substances. I. Computations from Nitrogen Isotherms. Washington, D.C., 1951; pp 373-380.

47. Taylor, H. E., *Inductively Coupled Plasma-Mass Spectrometry : Practices and Techniques*. Academic Press: San Diego, 2001.

48. Ishihara, T.; Kagawa, M.; Hadama, F.; Takita, Y., Copper Ion-Exchanged SAPO-34 as a Thermostable Catalyst for Selective Reduction of NO with C3H6. *Journal of Catalysis* **1997,** *169* (1), 93-102.

49. Hu, X.; Yang, M.; Fan, D.; Qi, G.; Wang, J.; Wang, J.; Yu, T.; Li, W.; Shen, M., The role of pore diffusion in determining NH3 SCR active sites over Cu/SAPO-34 catalysts. *Journal of Catalysis* **2016,** *341*, 55-61.

50. Ma, L.; Su, W.; Li, Z.; Li, J.; Fu, L.; Hao, J., Mechanism of propene poisoning on Cu-SSZ-13 catalysts for SCR of NOx with NH3. *Catalysis Today* **2015,** *245*, 16-21.

51. Zuo, Y.; Han, L.; Bao, W.; Chang, L.; Wang, J., Effect of CuSAPO-34 catalyst preparation method on NOx removal from diesel vehicle exhausts. *Chinese Journal of Catalysis* **2013,** *34* (6), 1112-1122.

52. Zheng, J.; Zhang, W.; Liu, Z.; Huo, Q.; Zhu, K.; Zhou, X.; Yuan, W., Unraveling the non-classic crystallization of SAPO-34 in a dry gel system towards controlling meso-structure with the assistance of growth inhibitor: Growth mechanism, hierarchical structure control and catalytic properties. *Microporous and Mesoporous Materials* **2016,** *225*, 74-87.

53. Lee, J.-F.; Lee, C.-K.; Juang, L.-C., Size Effects of Exchange Cation on the Pore Structure and Surface Fractality of Montmorillonite. *Journal of Colloid and Interface Science* **1999,** *217* (1), 172-176.

# 9.0 Appendixes

## Appendix 1: Additional XRD results

Figure A1, A.2 and A.3 shows the diffractograms of the additional samples. ConvS_02 had to be thrown away due to nothing left after filtration, so there does not exist a diffractogram of this sample.

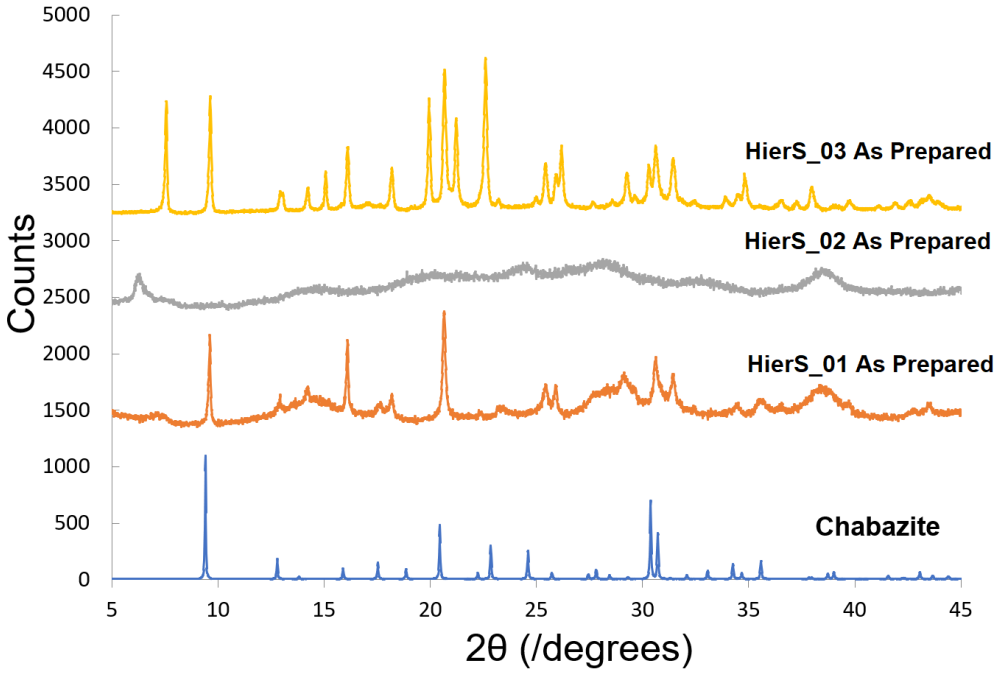


*Figure A.1: First bach of hierarchial SAPO-34 samples.*

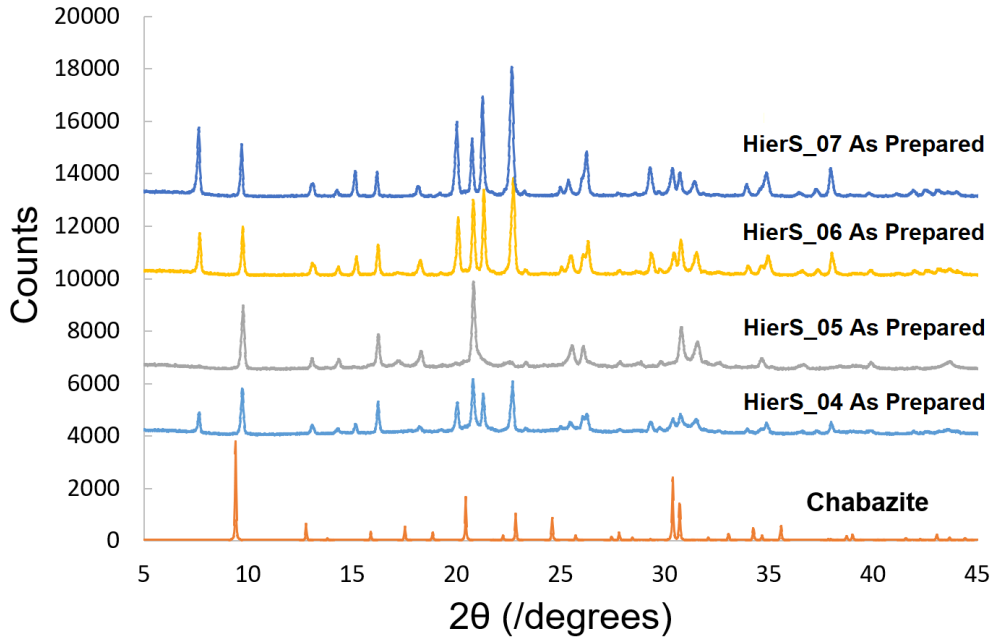


*Figure A.2: Second bach of hierarchial SAPO-34 samples.*

Figure A.3 shows the diffractograms of the additional as prepared CuSAPO-34.

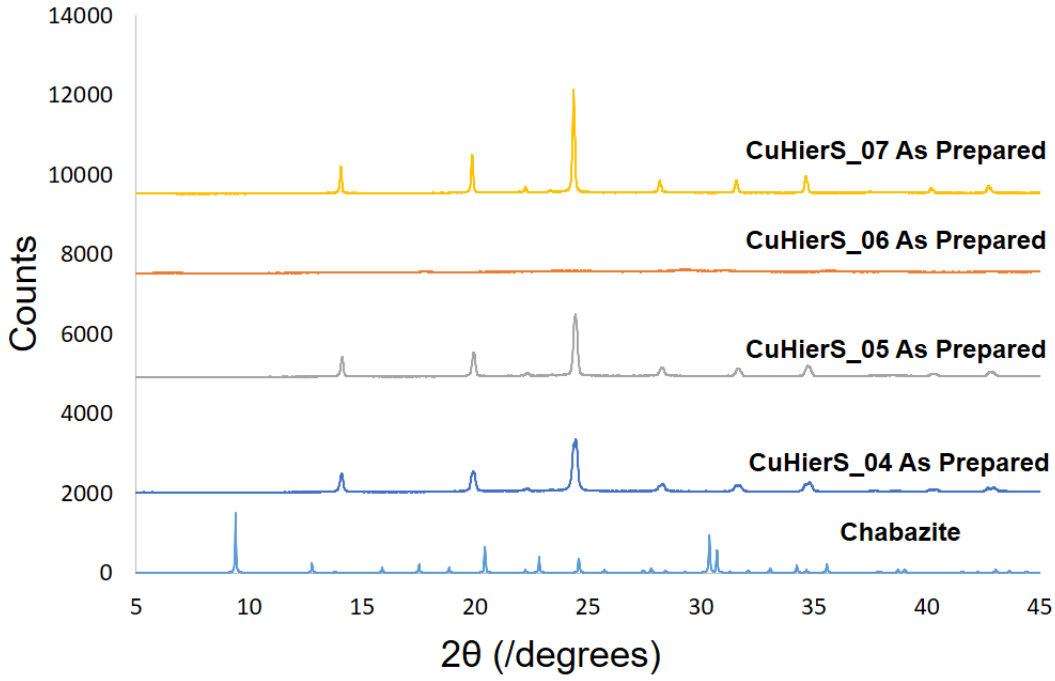


*Figure A.3: Second bach of hierarchial CuSAPO-34 samples.*

## Appendix 2: Additional BET results

Figure A.4 show linear isotherms for additional samples.

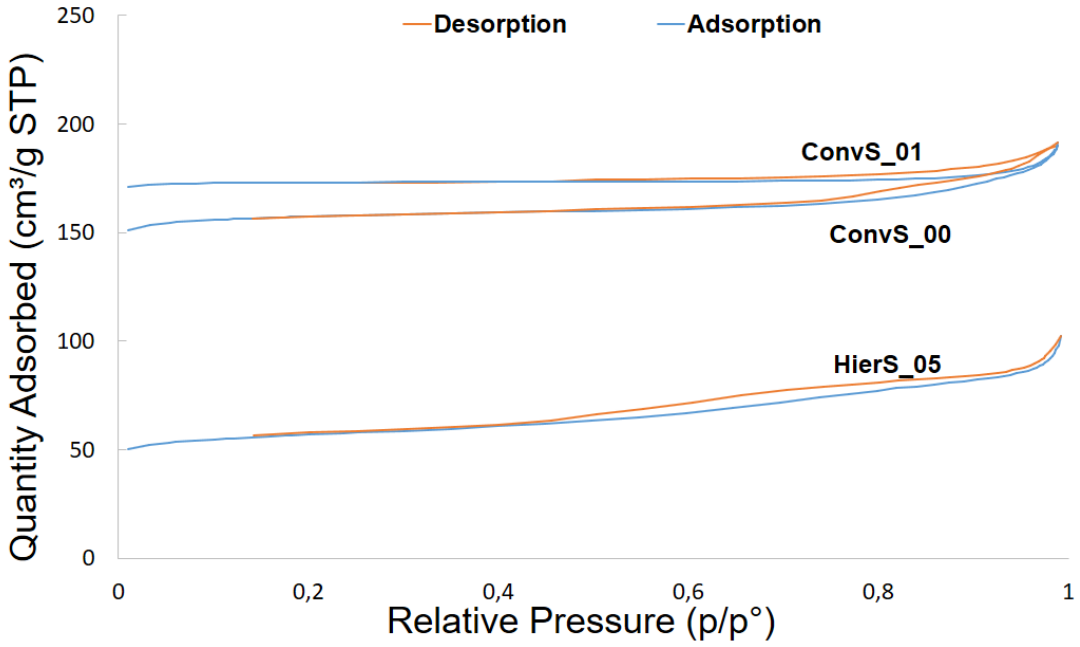


*Figure A.4: The linear isotherms for the three plains SAPO-34, ConvS_01, ConvS_00 and HierS_05.*

Figure A.5 shows BET specific surface areas, external area and micropore area of ConvS_00 and Cu:ConvS_00

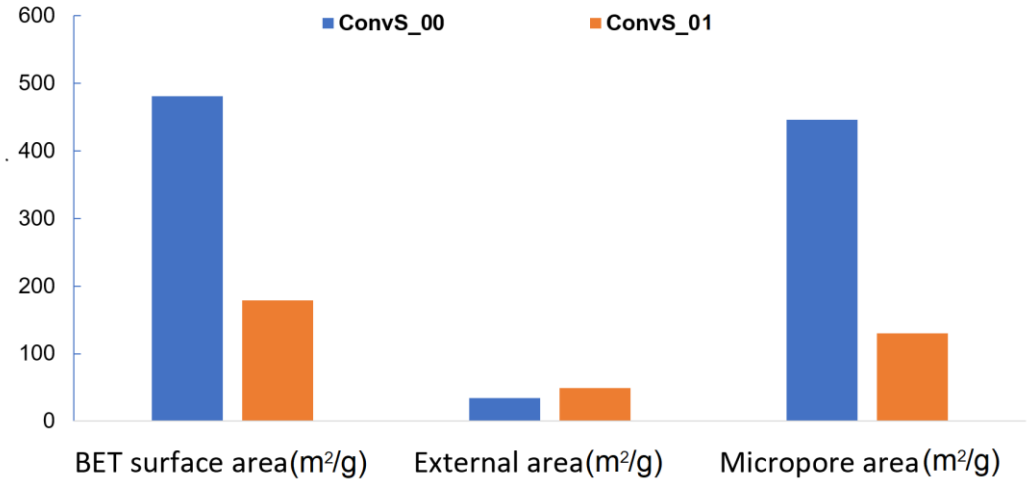


*Figure A.5: Surface area, external area and micropore area for the samples ConvS_00 and Cu:ConvS_00.*

Figure A.6 shows the pore size distributions for AgCu:ConvS_00D, Cu:ConvS_00, HierS_05 and ConvS_00.

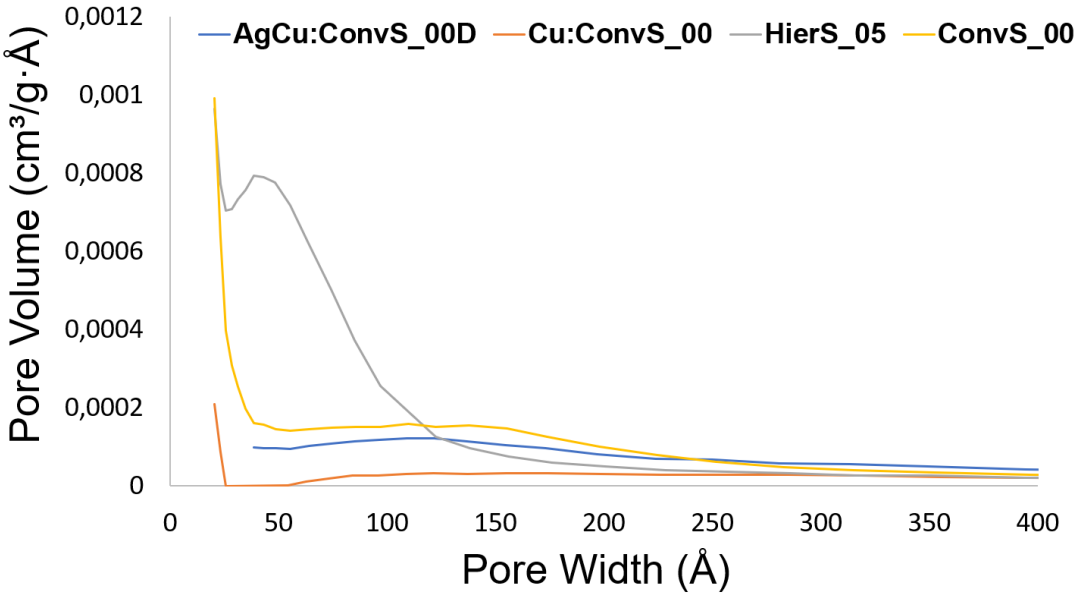


*Figure A.6: Pore size distribution for AgCu:ConvS_00D, Cu:ConvS_00, HierS_05 and ConvS_00.*